Geostrophic Turbulence

1 Introduction

Geostrophic turbulence provides the theoretical framework for understanding the nonlinear fluid dynamics of planetary circulations, as a complement, *e.g.,* to various flavors of large-scale wave dynamics and forced mean circulations such as the Hadley Cell or oceanic gyres. Because of different large-scale dynamical influences, many different simplified models for different phenomena have been devised.

In the ocean and atmosphere the majority of large-scale, extra-tropical motions (*i.e.,* mesoscale, synoptic scale, and planetary scale) are strongly influenced by rotation and stable stratification, with small values for Rossby, $Ro = V/fL$, and Froude, $Fr = V/NH$, numbers. This implies geostrophic and hydrostatic momentum balances at leading order, *viz.,*

$$fv_g = \phi_x, \quad fu_g = -\phi_y, \quad b = \phi_z\,, \tag{1}$$

where the subscript g denotes the geostrophic horizontal velocity. The leading-order asymptotic theory for the dynamics of this regime as $Ro, Fr \to 0$ is called *quasigeostrophy* (QG).

Much of the existing dynamical theory about the general circulation and its principal eddy variability (*e.g.,* turbulence) comes from QG theory, complemented of course by global General Circulations Models (GCMs) for weather, currents, material distributions and climate that themselves solve more fundamental fluid equations (usually the hydrostatic Primitive Equations). There is a healthy scientific tension between more complete theory in the simpler QG model and more realistic and complete simulations in the GCMs. The derivation of QG theory as an asymptotic expansion is a basic part of geophysical fluid dynamics (*e.g.,* explained in McWilliams (2006) and other textbooks).

The governing evolutionary equation for QG is

$$\frac{Dq}{Dt_g} = n.c.t.\,, \tag{2}$$

where q is the *QG potential vorticity*; D/Dt_g is the geostrophic advection operator with purely horizontal advection,

$$\begin{aligned} \frac{D}{Dt_g} &= \frac{\partial}{\partial t} + \mathbf{u}_g \cdot \nabla_h \\ &= \frac{\partial}{\partial t} + J(\psi,\ )\,; \end{aligned} \tag{3}$$

ψ is the rotational streamfunction for the horizontal geostrophic velocity (equal to $f^{-1}\phi$ in QG); ∇_h is the horizontal gradient operator; J is the horizontal Jacobian operator; and $n.c.t.$ denotes any non-conservative terms associated with forcing and dissipation. The QG model is completed by specifying the relation between q and ψ. This relation is a linear elliptic spatial operator that takes different forms in different regimes (listed below). The QG theoretical landscape, in particular for geostrophic turbulence behaviors, is a complicated one because scientists have found many different types of highly simplified models to be useful, and then worked extensively to compare among

these simplified models, applying Occam's razor to identify the most fundamental explanation as the simplest model in which an interesting result is found.

Barotropic (equivalent to 2D flow, whether uniformly rotating or not):

$$q \;=\; \zeta \;=\; \nabla_h^2 \psi \,. \tag{4}$$

This is the simplest model for the advective dynamics of geostrophic turbulence, with inverse energy cascade, forward enstrophy cascade and dissipation, coherent vortices, *etc.*

Planetary barotropic (with Coriolis frequency $f(y)$ varying with latitude, $\beta \;=\; df/dy \neq 0$; here $f_o \;=\; 2\Omega_e \sin[\theta]$ and $\beta \;=\; 2\Omega_e a_e^{-1} \cos[\theta]$, where Ω_e is Earth's rotation rate, a_e is Earth's radius, θ is the latitude, $y \;=\; a\theta$, and a Earth's radius; in the asymptotic expansion, it is assumed that $\beta L/f_o \;\sim\; Ro$):

$$q \;=\; f(y) + \zeta \;\rightarrow\; \beta y + \nabla_h^2 \psi. \tag{5}$$

In the final relation, for tidiness, we have subtracted the constant f_0 since it contributes nothing to (2) where q enters only with derivatives. This is the simplest model for examining the relation between advective cascades and Rossby waves.

Barotropic topographic (in a layer of mean depth H and variable bottom elevation $B(x,y)$; in the asymptotic expansion, it is assumed that $B_o/H \;\sim\; Ro$):

$$q \;=\; \frac{f_o}{H} B(x,y) + \nabla_h^2 \psi \,. \tag{6}$$

This is a different simple model for QG waves (here topographic waves, analogous to Rossby waves, based on the spatial gradient of the first term in q), turbulence, and non-uniform mean flows guided by topographic contours.

Shallow water or reduced gravity or equivalent barotropic: (or a layer with a deformable top or bottom "free-surface" interface, hence an associated radius of deformation, $R_d \;=\; \sqrt{\Delta \bar{b} H}/f_o \;=\; 1/\gamma$; in the asymptotic expansion, it is assumed that $L \;\sim\; R_d$ or, equivalently, that $Fr \;=\; V/\sqrt{\Delta \bar{b} H} \;=\; V/f_o R_d \;\sim\; Ro$:

$$q \;=\; \nabla_h^2 \psi - \gamma^2 \psi \,. \tag{7}$$

This is a simplest model for the combined effects of rotation and stratification (*i.e.,* gravitational force on the deformed free surface).

All of these "single-layer" QG models can be combined by additively including the different q terms.

3D QG: for a rotating, stratified fluid with $Fr \;\sim\; Ro$, or, equivalently, Burger number, $B \;=\; (N_o H/f_o L)^2 \;\sim\; 1$:

$$q \;=\; \nabla_h^2 \psi + \frac{\partial}{\partial z} \left(\frac{f_o^2}{N^2(z)} \frac{\partial \psi}{\partial z} \right) + \beta y \,. \tag{8}$$

This model can be formulated with flat, isothermal vertical boundaries with a $\partial_z \psi = 0$ boundary condition, in which case it is often called interior QG). Or it can be generalized with the kinematic boundary condition of no normal flow and a QG approximation of the buoyancy equation to include bottom topography at the mean level of the bottom,

$$w \;=\; -\frac{f}{N^2} \frac{D}{Dt_g} \partial_z \psi \;=\; J(\psi, B) \quad \text{at} \quad z \;=\; -H \,, \tag{9}$$

and/or the top-surface temperature condition at its mean level,

$$w \;=\; -\,\frac{f}{N^2}\,\frac{D}{Dt_g}\,\partial_z\psi \;=\; 0 \quad \text{at} \quad z \;=\; 0\,. \tag{10}$$

When $q = 0$ in the interior and the bottom is flat, then (10) is the only prognostic equation in what is called surface QG (see below).

The 3D QG model is the most "realistic" QG model because it includes vertical structure. It, and the other QG models discussed above, may or may not evolve in a way that remains consistent with is asymptotic derivation assumptions of small Ro and Fr. If it evolves to an inconsistent state, its solution may remain mathematically well behaved because Ro and Fr are not parameters in the QG model, but then the evolution in a more general model will depart from the QG evolution; ***e.g.,*** gravity waves may be spontaneously emitted. This is referred to as "QG-breakdown" or, more generally, as "limits of momentum-balanced evolution", and it will be discussed at the end of this chapter.

I have used an oceanic configuration here, with $-H \;\le\; z \;\le\; 0$, but there is an analogous atmospheric one with $0 \;\le\; z \;\le\; H$. Notice that (7) is a reduced form of (8) for a single vertical length scale, H, with R_d, $1/\gamma \;\sim\; NH/f_o$, but (7) clearly lacks the fully 3D dynamics with multiple, interacting vertical scales. This is the most complete QG model.

Surface QG (SQG:) The simplification of 3D QG with $q \;=\; 0$ in the interior using (8), the surface condition (10), and a semi-infinite domain with $H \;\to\; \infty$. This yields a different kind of "single-layer" QG model, which has a 2D evolutionary equation for the surface buoyancy field, $b = f^{-1}\partial_z\psi$, advected by the surface geostrophic velocity, as in (10). Then the 3D ψ field is calculated from the 3D $q - \psi$ relation (8) for zero q. SQG is most interesting because it has more active small-scale behavior (***i.e.,*** with shallower wavenumber spectra than the enstrophy inertial-range $E \;\sim\; k_h^{-3}$ of 2D turbulence) than do any of the other QG models, although it like the other QG models has a net inverse cascade of total, volume integrated energy, as explained below. A related interesting behavior in SQG is its tendency to generate surface buoyancy filaments somewhat like the surface fronts commonly found in both the atmosphere and ocean (Held ***et al.***, 1985). In some ways the emergence boundary fronts and filaments in SQG anticipates, albeit weakly, the breakdown of geostrophic turbulence (Sec. 9), while still staying within the geostrophic approximation.

An important property of all these geostrophic regimes, with their linear functional dependencies on ψ, is parity symmetry: the equations are unchanged by the transformation,

$$(\psi,\; y,\; B) \;\longrightarrow\; (-\,\psi,\; -\,y,\; -\,B)\,.$$

This means that cyclonic and anticyclonic eddies evolve in essentially equivalent ways. Violation of parity symmetry in measurements and simulations is often the simplest way to detect ageostrophic behavior.

Another important regime for geostrophic turbulence is its interaction with mean flow, which is relevant to the general circulations of the atmosphere and ocean; the equations for this problem can be obtained from any of the preceding models by substituting

$$\psi \;=\; \overline{\psi} + \psi', \quad q \;=\; \overline{q} + q', \quad \ldots\,. \tag{11}$$

This allows for turbulent fluctuations to arise from shear instabilities of the mean circulation. Within QG dynamics the only instability types are barotropic ($\nabla_h \overline{\psi} \neq 0$) and baroclinic ($\partial_z \overline{\psi} \neq 0$) or both.

The advective dynamics of these regimes is referred to, individually, as barotropic turbulence, β turbulence, topographic turbulence, shallow-water (or γ) turbulence, 3D geostrophic, and SQG turbulence and, collectively, as geostrophic turbulence. They have in common a single dependent variable (*e.g.,* ψ); a first-order PDE in time (which implies that QG has no inertia-gravity waves); a spatially second-order, elliptic linear differential $q[\psi]$ relation; and advection only by the non-divergent, horizontal, geostrophic velocity. They also have two quadratic inviscid invariants, energy and (potential) enstrophy. The relevant forms of energy are

$$\begin{aligned} E &= \int\int d\mathbf{x}_h \, \frac{1}{2} (\nabla_h \psi)^2 \,, \\ &= \int\int d\mathbf{x}_h \, \frac{1}{2} \left[\, (\nabla_h \psi)^2 + \gamma^2 \psi^2 \, \right] \,, \text{ and} \\ &= \int\int\int d\mathbf{x} \, \frac{1}{2} \left[\, (\nabla_h \psi)^2 + \frac{f_o^2}{N^2(z)} \left(\frac{\partial \psi}{\partial z} \right)^2 \, \right] \,, \end{aligned} \tag{12}$$

for (4)-(6), (7), and (8), respectively. For SQG the energy is the same as for 3D QG, although often attention is focused on just the surface component of the energy,

$$E_0 = \int\int d\mathbf{x}_h \, \frac{1}{2} \left(\, (\nabla_h \psi)^2 + \frac{f_o^2}{N^2(z)} \left(\frac{\partial \psi}{\partial z} \right)^2 \, \right) \Big|_{z=0} \,, \tag{13}$$

Notice the presence of both a kinetic and an available potential energy in many of these models. The relevant form of enstrophy is the domain integral of q^2 in all cases, although for β and topographic turbulence there is an alternative form with the environmental contribution (*i.e.,* βy or $f_o B(x,y)/H$) subtracted from q before it is squared. Because of the simple form in (2), the domain integral of any functional of q is also an inviscid invariant of geostrophic turbulence. As with 2D flow, the existence of two independent, quadratic conservative invariants implies that there are inverse-energy and forward-enstrophy inertial-range turbulent cascades. The non-diffusive invariants for a horizontally advected passive tracer field, c, are identical to those for q in the geostrophic models; so we expect a forward tracer cascade to dissipation analogous to the enstrophy cascade in 2D and geostrophic turbulence. In the SQG model there is an inertial range with a spectrum $E_0(k_h) \propto k_h^{-5/3}$, which has the interesting, non-intuitive behavior of simultaneous forward cascade of surface available potential energy and inverse cascade of surface kinetic energy (Capet *et al.*, 2008a; Sec. 8).

The analogies between 2D and geostrophic turbulence are quite strong, including the cascade behaviors just mentioned. Geophysical examples of large-scale energy spectra, consistent with the k^{-3} enstrophy inertial range, were shown in the chapter, *2D Homogeneous Turbulence*; we will see below that this inertial-range spectral form is also valid for geostrophic turbulence. Again by analogy with 2D turbulence, we expect coherent vortices to develop in geostrophic turbulence. However, both the β and topographic models — as well as all of the models when $\nabla_h \overline{q} \neq 0$ — contain QG wave solutions (*e.g.,* Rossby waves) that can compete with, and sometimes disrupt, the advective behavior in geostrophic turbulence.

2 Rotating, Uniform-Density Turbulence

Within the geostrophic approximation, uniform background rotation plus uniform density are a cause of 2D dynamics, hence 2D turbulence. This is a consequence of the Taylor-Proudman theorem, whereby the only hydrostatic, geostrophic horizontal flows are barotropic, *i.e.,* $\partial_z \mathbf{u}_h = 0$. However, in a 3D, uniform density fluid with strong rotation, there can be additional phenomena that arise either in addition to or *en route* to 2D dynamics:

Inertial waves and 3D adjustment: A 3D initial condition will undergo a geostrophic adjustment process to a barotropic state, partly through emission of ageostrophic inertial waves (Davidson *et al.*, 2006) and partly through a more advective and dissipative evolution (Smith and Waleffe, 1999).

Centrifugal instability: A flow that is centrifugally unstable (*e.g.,* because $f+\zeta$ changes sign in the domain) will undergo a 3D ageostrophic instability before adjusting to a barotropic state that is centrifugally stable (Kloosterziel and Carnevale, 2008). This can lead to an asymmetric barotropic state with stronger cyclones than anticyclones.

Vertical boundary layers and forcing: If there are vertical boundaries, there will be Ekman boundary layers. With small Ro usually their effect will be simply to provide a near-boundary vortex stretching through Ekman pumping that has the effect of damping the barotropic flow; *e.g.,*

$$\partial_t \zeta + \ldots \; = \; -R\zeta \,, \tag{14}$$

with damping time R^{-1} (McWilliams, 2006). This effect is commonly included in single-layer QG turbulence. If there is strong forcing at the boundary, then the Ekman layer dynamics can be sufficiently nonlinear that its vortex stretching generates stronger barotropic cyclones than anticyclones, possibly in combination with the selection mechanism of centrifugal instability (McEwan, 1976); however, this behavior lies outside strictly geostrophic dynamics.

3 Free Surface and Finite R_d

The QG model, (2), (3), and (7), can be rewritten as

$$\frac{\partial}{\partial t}[\nabla_h^2 \psi - \gamma^2 \psi] + J(\psi,\, \nabla^2 \psi) \; = \; n.c.t. \,, \tag{15}$$

since the geostrophic advection of the second term in (7) is trivial (*i.e.,* $J(\psi,\psi) \;=\; 0$). For $L \ll 1/\gamma$, the equation is again the same as for 2D flow. An initial state on this scale L will undergo an inverse energy cascade, coherent vortices will emerge, and L will grow. When it reaches $L \approx 1/\gamma$, the far-field velocity associated with local concentrations of q begin to have a much smaller reach, since the Helmholtz operator in (7) has an exponentially decaying Greens function, *i.e.,* with $V(r) \;\sim\; e^{-\gamma r}$ for large r instead of the algebraically decaying solution, with $V \;\sim\; 1/r$, for the Poisson operator in (4). This diminishes the distant interactions among the

vortices and provides a degree of cascade arrest for the flow evolution; here, however, the dynamics of the arrest is horizontally isotropic, unlike with β (Sec. 4).

If the flow has $L \gg 1/\gamma$, then the approximate form of (15) is

$$\frac{\partial \psi}{\partial t} - \gamma^{-2} J(\psi,\ \nabla^2 \psi) \ \approx \ n.c.t.\,, \tag{16}$$

which implies a much slower rate of evolution than in 2D turbulence. In 2D flow the advective operator causes an evolutionary tendency,

$$\begin{aligned} \nabla^2 \psi_t \ &= \ -J(\psi,\ \nabla^2 \psi) \\ \Rightarrow \ \psi_t \ &\sim \ \psi^2/L^2 \ \sim \ V^2 \ \sim \ E\,, \end{aligned} \tag{17}$$

whereas a similar estimate for (16), using (12), is

$$\begin{aligned} \psi_t \ &= \ \gamma^{-2} J(\psi,\ \nabla^2 \psi) \\ \Rightarrow \ \psi_t \ &\sim \ \psi^2/\gamma^2 L^4 \ \sim \ (\gamma L)^{-2} E\,, \end{aligned} \tag{18}$$

which is very much slower when $\gamma L \gg 1$. Note also that the potential vorticity relation (7) becomes

$$q \ \approx \ -\gamma^2 \psi \tag{19}$$

in this regime, which implies that the leading-order expressions for both energy and enstrophy are no longer independent, hence that their turbulent cascades no longer need to be in opposite directions in wavenumber space.

An illustration of the free evolution of γ turbulence is in Fig. 1, for the regime $L \gg 1/\gamma$ (Larichev and McWilliams, 1991). The coherent vortices are approximately axisymmetric, but they are no longer spatially sparse (hence their kurtosis is not as large as in 2D flow). A typical separation distance is $1/\gamma$ (*i.e.,* a far-field velocity decay scale), which is much smaller than a typical vortex size, L. The inverse cascade continues, albeit at the slower (partially arrested) rate discussed above. With time the coherent vortices become fewer and larger, through merger interactions, and even slightly sparser. Filamentation is much less prevalent here compared to 2D turbulence — even during vortex mergers — in association with the fact that (16) is different from the classical scalar advection equation,

$$\frac{\partial c}{\partial t} + J(\psi,\ c) \ \approx \ n.c.t.,\tag{20}$$

which applies in 2D turbulence to $c \ = \ q \ = \ \zeta$.

The horizontal streamfunction pattern of the coherent structures in γ turbulence for $L \gg 1/\gamma$ (Fig. 1) resembles closely that of the pancake vortices in 3D stratified turbulence. In both instances it is the dominant influence of stable stratification that is controlling this structure. The mechanism for how this works is clearer for γ turbulence, where the Helmholtz operator in (7) provides the connection between the advectively preserved potential vorticity field and the advecting velocity field; in stratified turbulence, the Ertel potential vorticity is a nonlinear functional of ψ, which makes the analysis more difficult.

In summary, we learn from γ turbulence that the geostrophic turbulent evolution will be slower on scales larger than R_d and that the spatial isolation of the coherent vortices will be less pronounced, compared to an equivalent 2D turbulence evolution.

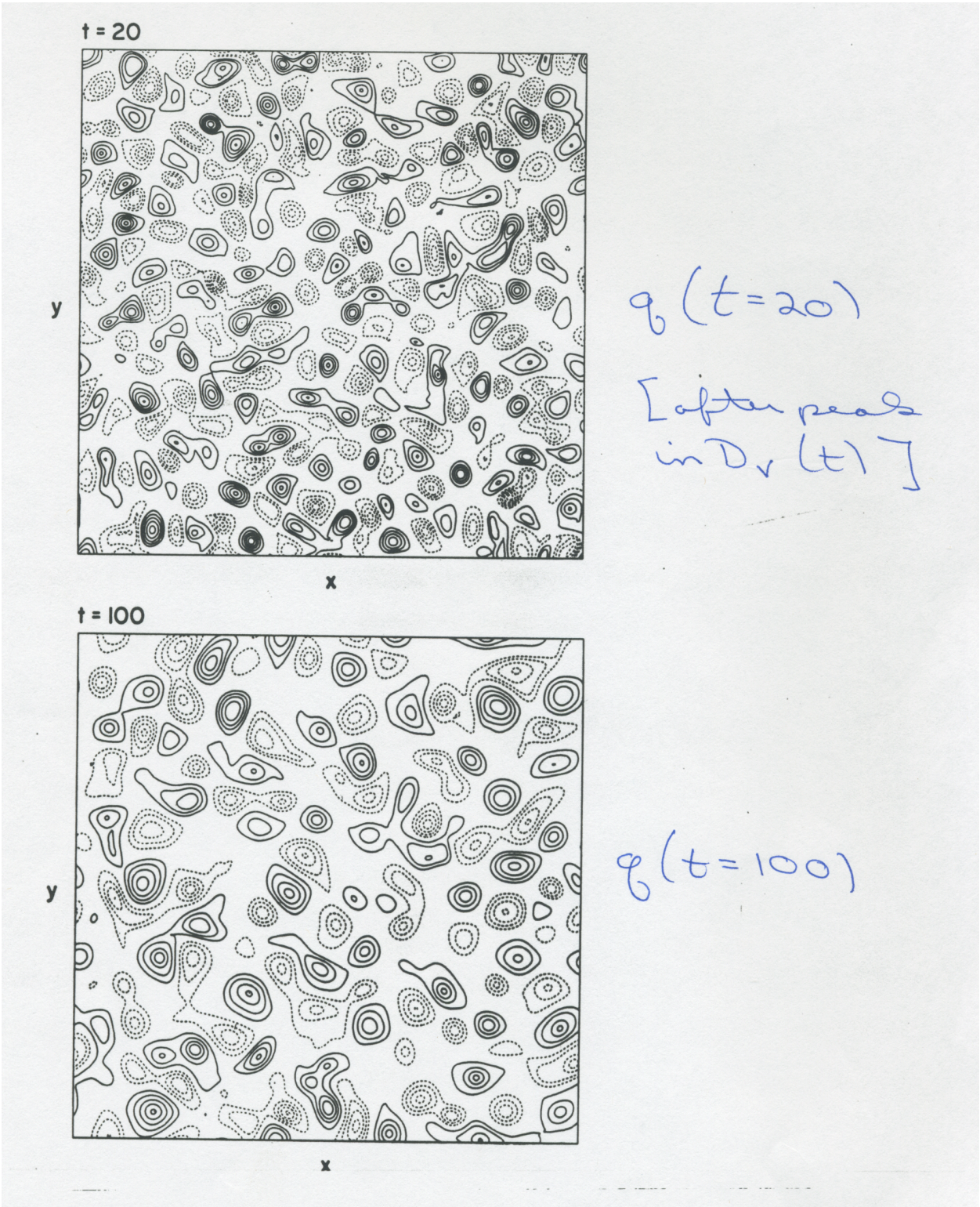

Figure 1: $q \approx -\gamma^2\psi$ fields at two times during the free evolution in shallow-water turbulence with large Re from random initial conditions with $\gamma \gg 1$ (Larichev and McWilliams, 1991).

There are interesting asymmetries that arise between coherent cyclones and anticyclones in rotating shallow-water models that have finite Ro values, in particular the dominance of anticyclones (Polvani *et al.*, 1994; Graves *et al.*, 2006).

4 β and Zonal Jets

The QG planetary model, (2)-(5), can be rewritten as

$$\frac{\partial \nabla^2 \psi}{\partial t} + J(\psi,\ \nabla^2 \psi) + \beta \frac{\partial \psi}{\partial x} \ = \ n.c.t. \tag{21}$$

Thus, the only addition to 2D fluid dynamics is the final l.h.s. term. It permits non-trivial linear inviscid solutions, called Rossby waves. For an unbounded domain, plane traveling waves have the normal-mode dispersion relation,

$$\sigma \ = \ - \frac{\beta k^x}{(k^x)^2 + (k^y)^2} \,, \tag{22}$$

where (k^x, k^y) is the horizontal wavenumber and σ is the frequency. 2D turbulence is horizontally isotropic and homogeneous in its symmetries. The presence of β breaks the isotropy symmetry, because it contributes only an x derivative in (21); this is also evident in the anisotropic Rossby propagation implied by (22).

For a given amount of energy, $E \ \sim \ \frac{1}{2} V^2$, the Rossby number, $Ro \ = \ V / f_o L$, will become smaller than the equivalent measure of the evolutionary rate for Rossby waves (*i.e.,* the frequency), $\beta L / f_o$, if L becomes sufficiently large, *i.e.,* $L > L_\beta$, where

$$L_\beta \ = \ \sqrt{V/\beta} \,. \tag{23}$$

Alternatively stated, L_β is the length scale for which the magnitudes of the 2nd and 3rd l.h.s. terms in (21) are the same. Since the inverse energy cascade in 2D turbulence (*i.e.,* in the approximation to (21) when $L \ll L_\beta$) acts to increase L while preserving V, we can therefore expect that small-scale initial conditions or forcing will evolve towards a larger-scale state where the β term becomes important (Rhines, 1975).

The effect of the waves is to cause dispersive propagation, so that the nonlinear interactions of the advective operator are "de-correlated" and thus made ineffective for turbulent cascading. This interferes in particular with the inverse energy cascade, causing a *cascade arrest*at $k \approx L_\beta^{-1}$, which also implies an arrest of the forward enstrophy cascade and the spectrum broadening in k (*cf.,* the argument presented in the *2D Homogeneous Turbulence*). (The term cascade arrest is used loosely to imply a decrease in the transfer rate of variance between scales, relative to the default expectation that a significant amount of transfer occurs during each typical eddy turnover time.) Dispersion also interferes with the coherent vortex dynamics, since wave dispersion destroys any spatial patterns in the flow. (Interestingly, a strong vortex, with $|\zeta| \ \gg \ \beta L$, is not destroyed by dispersion in (21), since a soliton-like balance between dispersive spreading and nonlinear steepening arises; however, a weak vortex cannot resist the dispersive spreading.) We can express this wave-advection competition in terms of the characteristic evolutionary rates, σ and L/V. The latter is anisotropic from (22), with $\sigma \to 0$ as $\mathbf{k} \to k^y \hat{\mathbf{y}}$. Therefore, the cascade

arrest is directionally dependent, as indicated in Fig. 2: the inverse cascade can proceed farther towards $\mathbf{k} = 0$ in k^y than in k^x, so the solution becomes increasingly anisotropic on large-scales, with $u \gg v$ since $\hat{u} = -ik^y\hat{\psi}(k^x, k^y)$ has more energy at $k^y < L_\beta^{-1}$ than $\hat{v} = ik^x\hat{\psi}(k^x, k^y)$ has at $k^x < L_\beta^{-1}$.

Thus, the outcome of a β cascade arrest is the development of primarily zonal flows, which alternate in direction on a y scale $\approx L_\beta$ (Fig. 2). Notice that $(u = u(y),\ v = 0)$ is an inviscid stationary state in (21), since it is a particular example of $J(\psi,\ q) = 0$. This behavior is illustrated in Figs. 3-5 for solutions of β turbulence on a sphere, which are in an equilibrium balance between random forcing and dissipation. Solutions are shown with different planetary rotation rates, and the outcome is a set of increasingly strong and narrow zonal jets as the rotation rate becomes larger (Nozawa and Yoden, 1997). This anisotropic cascade arrest and evolution towards zonal jets has been suggested as the explanation for Jupiter's jets in its stably stratified superficial layer (*i.e.,* its "stratosphere"), with interior deep convection as the excitation source for the turbulence. It also is considered relevant to Earth's zonal jets, the atmospheric westerlies, and the Antarctic Circumpolar Current (ACC), by acting to accentuate the horizontal anisotropy and limit the meridional width to $L \sim L_\beta$; however, there does not seem to be quite enough room on Earth — or too much kinetic energy or too slow a planetary rotation rate for L_β to be small enough — to be in the regime of multiple jets, except possibly marginally so in the ACC.

There is a large literature on barotropic and shallow-water flows on a rotating sphere, primarily motivated by relevance to the visible flows on the gas giant planets. Williams (1978) was the first to show the possibility of the spontaneous development of alternating zonal flows. A particular question in this subject is whether the equatorial flow should be westward or eastward (*i.e.,* super-rotation with flow faster than the planet's rotation). On gas giants equatorial super-rotation is the dominant observed behavior. The present understanding from this class of models is that super-rotation can be a random outcome of initial conditions, but it is assisted by thermal damping (Scott and Polvani, 2008).

The competition between coherent vortices and zonal jets is illustrated in Fig. 6 for numerical solutions of β turbulence in a periodic square (McWilliams, 1984). The initial conditions are random with a spectrum peak at $k_0 > k_\beta$. The early evolution is as in 2D turbulence, with coherent vortices emerging and leading to increasing spatial intermittency, as indicated here by the vorticity kurtosis. When $k_0 \gg k_\beta$, the vortices become well defined on a sufficiently small scale such that the β effect on them is weak; in this case, they emit weak Rossby-wave radiation wakes as they propagate and mutually interact (*e.g.,* merge), and the kurtosis ceases to grow after having reached a large value. On a very, very long time scale, much longer than plotted here, we can expect the inverse cascade to continue until the solution eventually turns into zonal jets with arrested cascades. In contrast, when k_0 is only modestly larger than k_β, the developing vortices (and initially growing kurtosis) are substantially influenced by β and experience sufficient dispersion that the kurtosis collapses shortly thereafter and the cascade arrests and jet configuration is achieved much more quickly.

Another behavior in β-turbulence is generation of mean flows due to spatial inhomogeneity in the forcing. When Rossby waves are emitted from a localized forcing zone in a zonally unbounded or periodic domain, then an eastward mean flow develops there, while westward mean flows develop in the far-field where the Rossby waves are damped (Haidvogel and Rhines, 1983). This effect occurs even when the flows are strongly turbulent. This process is invoked to explain

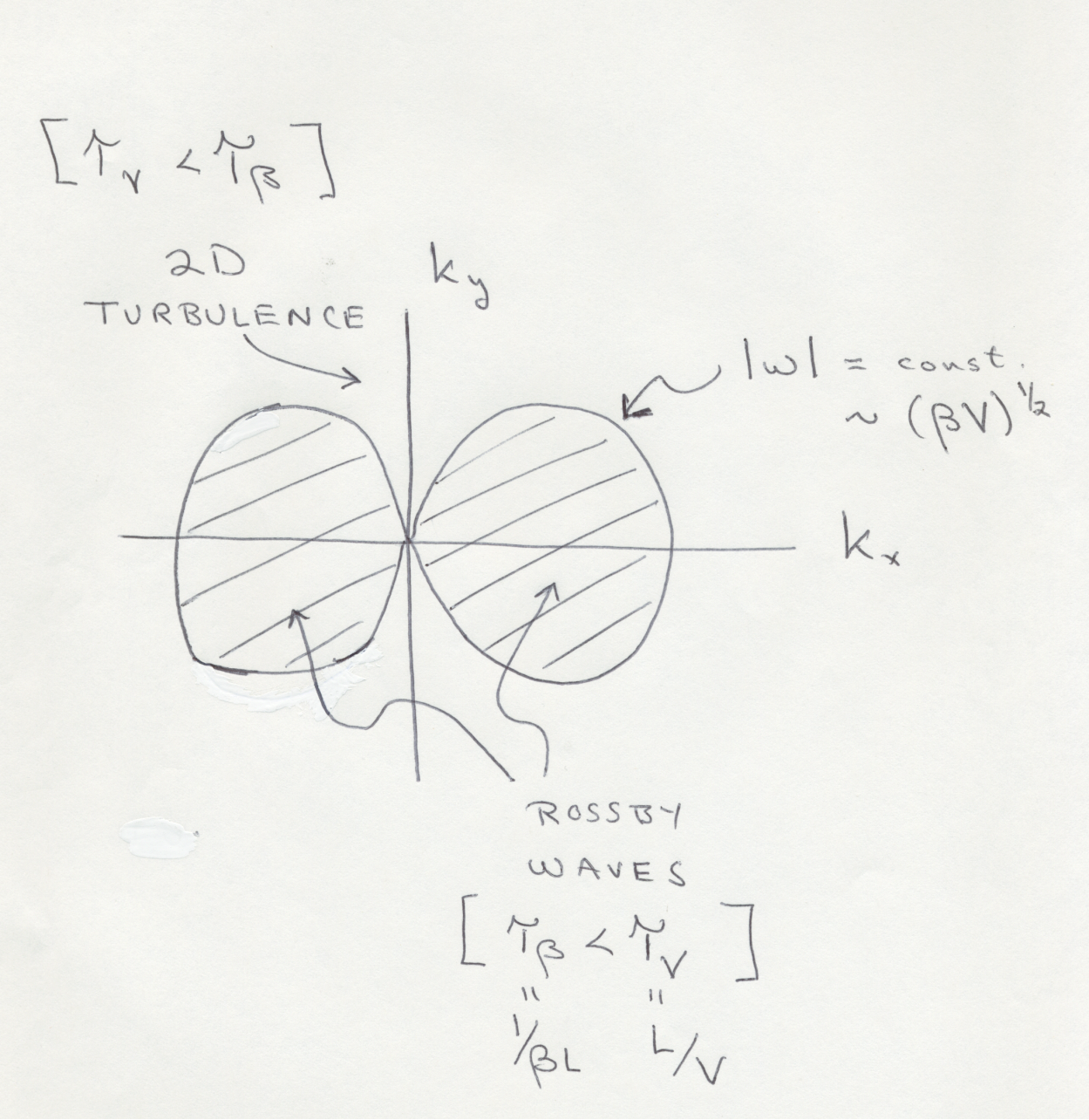

Figure 2: Sketch of the wavenumber-space regimes in β-turbulence.

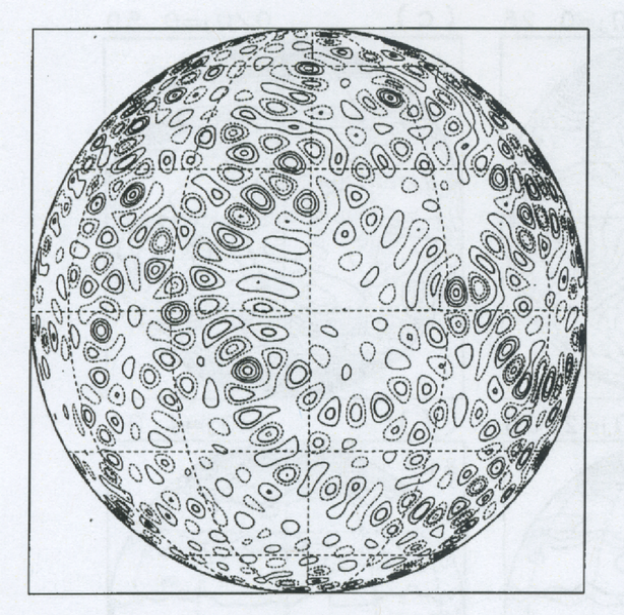

Figure 3: Instantaneous realization of the random vorticity forcing field for barotropic flow on a rotating sphere. (Nozawa and Yoden, 1997)

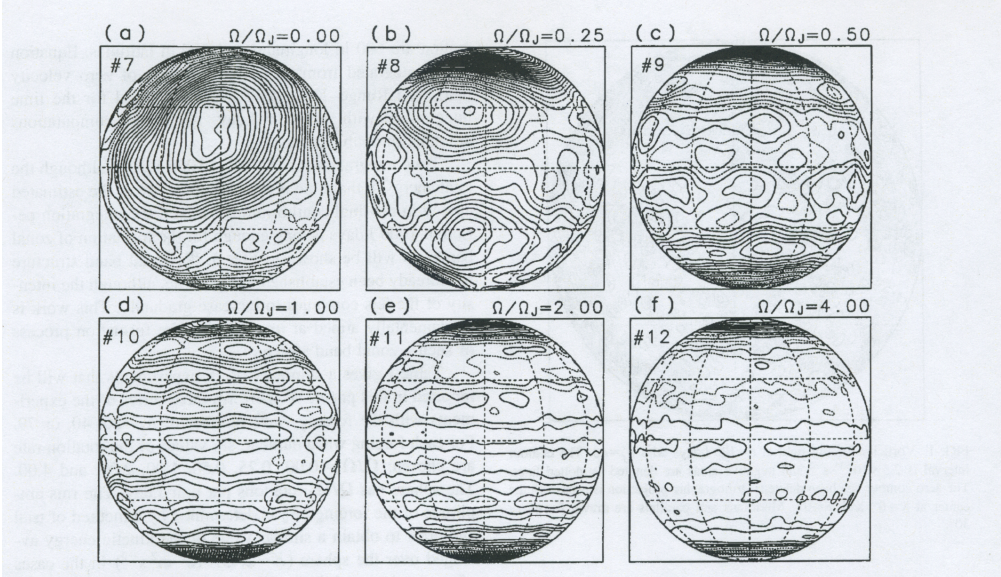

Figure 4: Instantaneous streamfunction field for barotropic flow on a rotating sphere with different values of a non-dimensional planetary rotation rate, Ω/Ω_J, that indicates the relative importance of β. (Nozawa and Yoden, 1997)

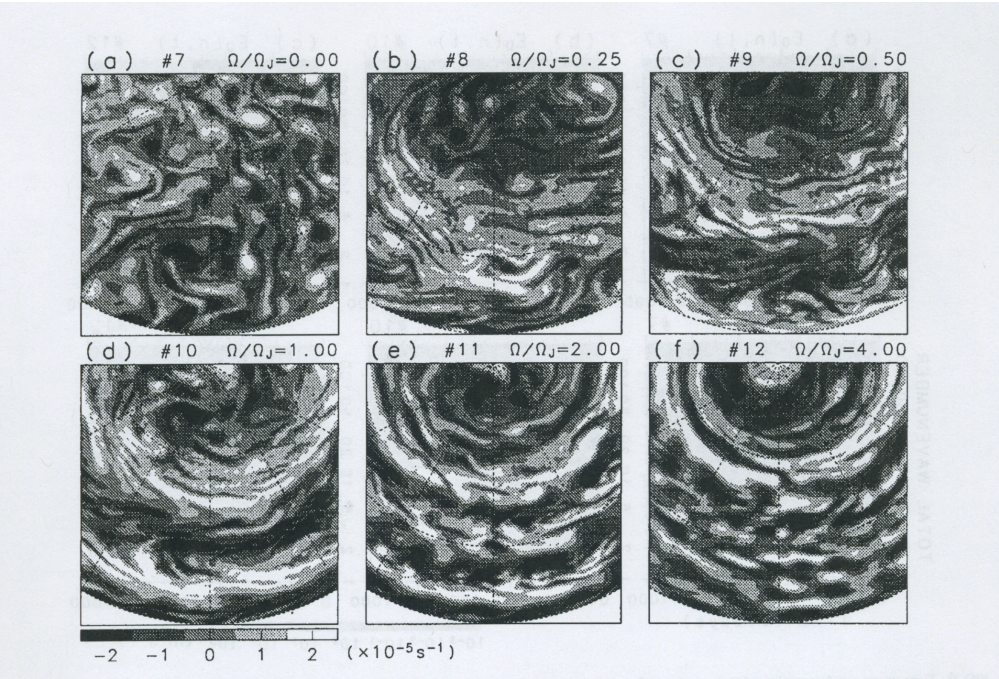

Figure 5: Instantaneous relative vorticity field for the same cases as in Fig. 4. Notice the disappearance of coherent vortices with increasing $\Omega//\Omega_J$. (Nozawa and Yoden, 1997)

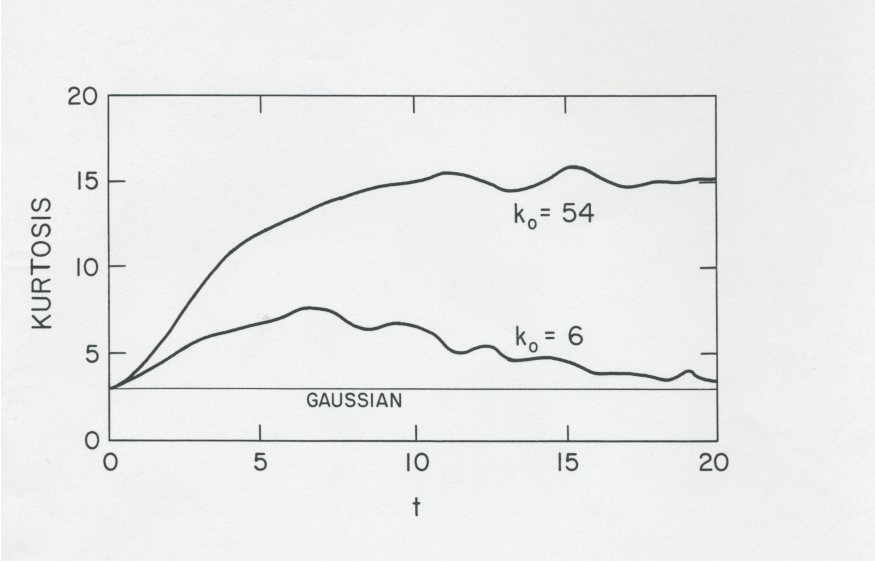

Figure 6: Evolution of the kurtosis (a measure of coherent vortex dominance) in freely evolving β-turbulence for $k_\beta = \sqrt{5}$ and two different values of the initial vorticity spectrum peak, k_o. (McWilliams, 1984)

the sharp peak in the atmospheric westerly wind jet or equatorial super-rotation (eastward mean flow). With sustained small-scale random forcing and a large β influence, 3D geostrophic flows on a sphere evolve until most of the energy is in the barotropic mode (see 6 below), and then inverse cascade transfers the kinetic energy to very large scales with strong anisotropy favoring zonal flows, albeit slowly because of inhibition of advective effects once the flow is strongly anisotropic due to β; *i.e.,* such flows exhibit only a partial cascade arrest until the large-scale energy sink (*e.g.,* bottom drag) establishes an equilibrium balance. The latter stages of this evolutionary sequence is often called *zonostrophic turbulence* (Galperin *et al.*, 2008). The predicted large-scale inertial range has an energy spectrum,

$$E(n) \sim \beta^2 n^{-5}\,, \tag{24}$$

where n is the total wavenumber index in a spherical geometry. This is much steeper than the than the $n^{-5/3} \sim k^{-5/3}$ inverse energy cascade spectrum predicted for 2D and 3D geostrophic turbulence without β. Fig. 7 illustrates the evolutionary pathway described above and some computational solutions that somewhat support the prediction in (24). This regime is considered more relevant to large, rapidly rotating planets, such as Jupiter, than to Earth.

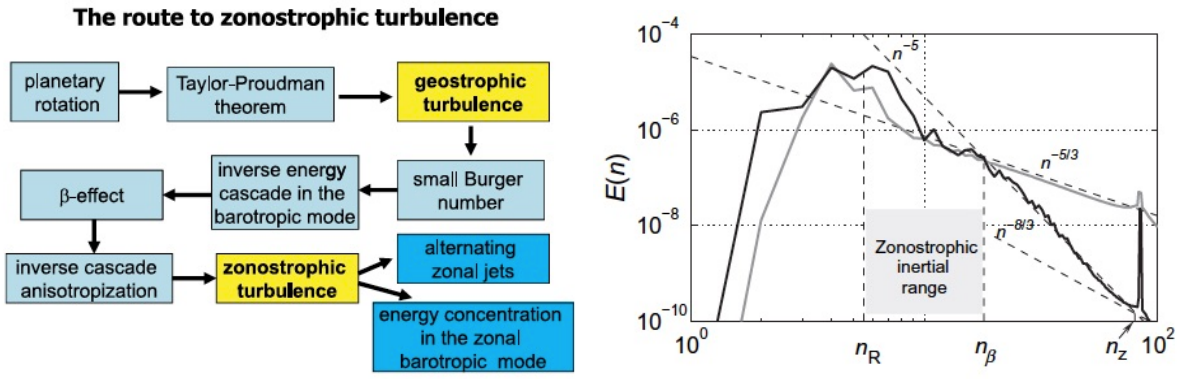

Figure 7: (Left) Schematic representation of physical processes leading from geostrophic to zonostrophic turbulence. (Right) The kinetic energy spectra for the equilibrium regime of zonostrophic turbulence. The black and gray lines show the zonal-velocity and residual spectra, respectively. n is the total spherical wavenumber index. $n_R \propto L_\beta^{-1}$ and $n_\beta \propto (\beta^3/\varepsilon)^{1/5}$. The inverse cascade is limited here by the combination of β-arrest and bottom drag. (Galperin *et al.*, 2008)

In summary, we learn from β turbulence that planetary-scale flows are likely to have an important Rossby wave component in their otherwise nonlinear dynamics, and often there will be a peak in the energy spectrum near $L = L_\beta$ and the emergence of quasi-stationary zonal jets, possibly followed by a slow further inverse cascade to $L \gg L_\beta$ if there is room on the rotating planet.

5 Topographic Turbulence

The QG model, (2), (3), and (6), can be rewritten as

$$\frac{\partial \nabla^2 \psi}{\partial t} + J(\psi,\, \nabla^2 \psi) + \frac{f_o}{H} J(\psi,\, B) \;=\; n.c.t. \tag{25}$$

This equation is equivalent to that of β turbulence for the particular topography $B(y) = H\beta y/f_o$ (*i.e.,* a uniform bottom slope upwards to the north in the northern hemisphere), but it has a richer dynamics for a more general $B(x, y)$. The largest scales of the topography, therefore, will influence the turbulence analogously to the β influence, leading to a cascade arrest, (topographic) Rossby waves, horizontal anisotropy, and along-slope jet flows.

The inviscid stationary states of (25) correspond, as usual, to $J(\psi,\ q) = 0$, or to

$$\zeta + \frac{f_o}{H} B = \mathcal{G}[\psi] \tag{26}$$

here, for any functional $\mathcal{G}$. For any smooth B and an initially small-scale flow field, (25) will imply approximately the same behavior as in 2D turbulence, including an inverse energy cascade to larger scale. If the scale becomes large enough, so that ζ is negligible in (26), then the inviscid stationary states satisfy

$$B \approx \mathcal{G}[\psi]\,, \tag{27}$$

which is flow along topographic contours. These states thus represent possible arrested states for the turbulent evolution, should it somehow achieve them. The evidence from computational solutions is that it often does; see Fig. 8.

A heuristic theory for this (Bretherton and Haidvogel, 1976) is based on the observation that turbulent cascades act to diminish the enstrophy through dissipation at small scales while preserving the energy, in flows that have both quantities as inviscid invariants; *i.e.,* the energy, here

$$E = \int\int d\mathbf{x}_h\, \frac{1}{2}(\nabla_h \psi)^2\,, \tag{28}$$

is a rugged invariant (*i.e.,* preserved for $Re \gg 1$), while the enstrophy,

$$Z = \int\int d\mathbf{x}_h\, \frac{1}{2}(\zeta + \frac{f_o}{H} B)^2\,, \tag{29}$$

is not. In 2D turbulence, the only way to diminish Z is by diminishing $|\zeta|$, but here it can also occur by developing a correlation

$$\zeta \approx -\frac{f_o}{H} B\,, \tag{30}$$

which, insofar as $\psi \sim -\zeta/L^2$, also resembles the relations (26) and (27). Thus, enstrophy dissipation and inverse cascade can combine to push the solution towards an arrested state.

The hypothesis that the flow achieves a state of minimum enstrophy for a given (initial) energy leads to a well posed problem in the calculus of variations. Its answer is the relation (26) for $\mathcal{G}$ a linear functional, $\mathcal{G}[x] = ax + b$ for a, b constants. This yields a linear elliptic boundary-value problem for ψ given B, whose solution has particular versions of the properties (27) and (30). (In the case of 2D turbulence, this state is a pair of opposite-sign vortices on the largest available scale of the domain, which is at least qualitatively similar to the late-time end-state discussed in that chapter.) One arrives at the same answer by making an alternative hypothesis of maximizing the "information entropy", $S = \int\int d\mathbf{x}_h\, |q| \log |q|$, and thus associating this theory with equilibrium statistical mechanics (but the question of why S should govern the evolution is subtle, and for me ultimately unsatisfying). Computational solutions exhibit a qualitative similarity to this prediction

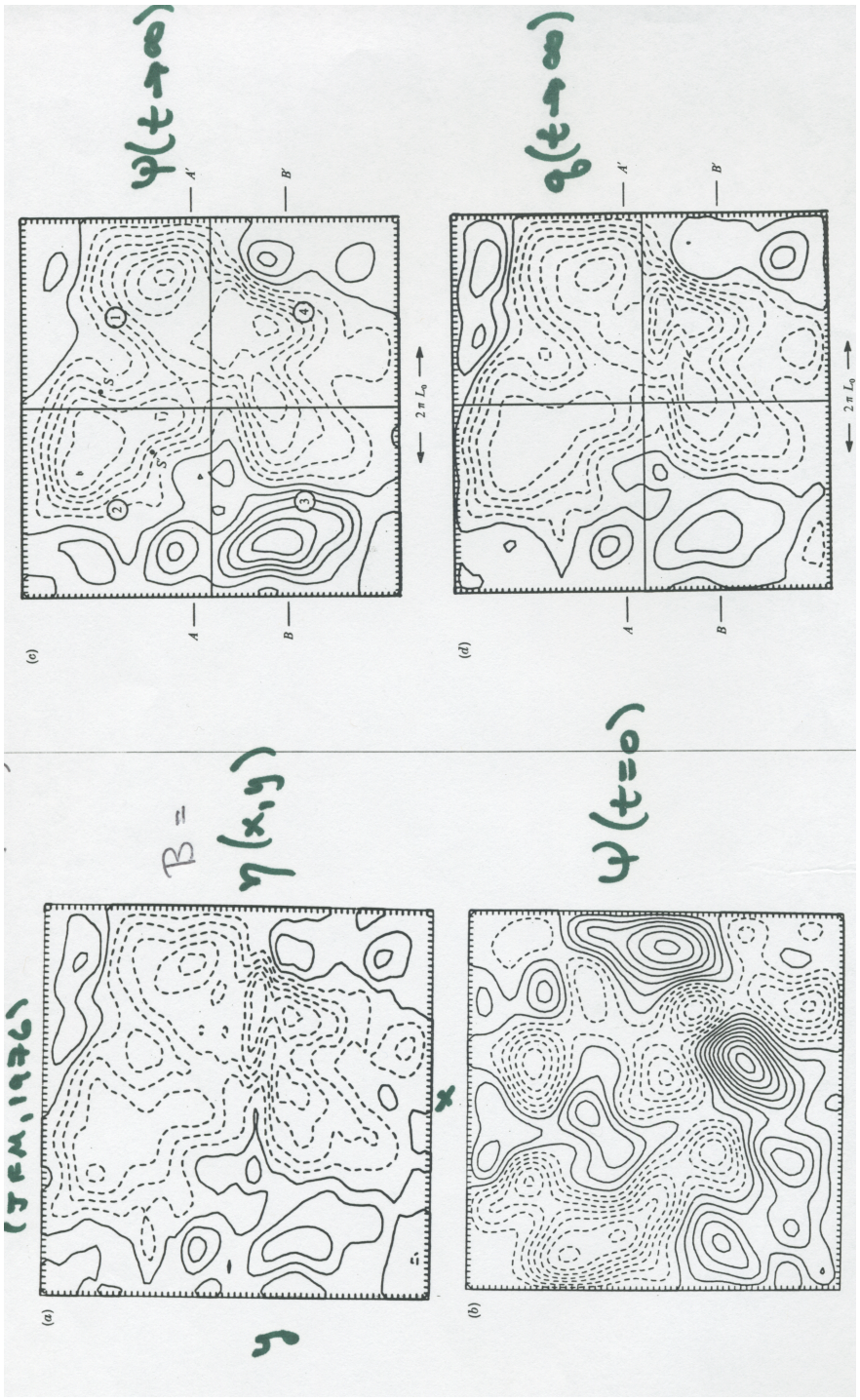

Figure 8: Freely evolving topographic turbulence: (a) is the topographic height, $B(x, y)$. (b) is the initial $\psi(x, y)$. (c) is the late-time ψ. (d) is the late-time potential vorticity q. Notice the strong correspondence between (a) and (d). (Bretherton and Haidvogel, 1976)

in their late-time configuration; however, the correspondence is not exact: flows satisfying (26) often occur with a $\mathcal{G}$ different than a linear functional and with different "branches" of $\mathcal{G}$ in different spatial regions. If the flow satisfies (26), then there is no further nonlinear tendency to evolve to a state with lesser Z or greater S. A particular version of this end-state is for cyclonic flow (*i.e.,* with vorticity of the same sign as f) around the rim of an ocean basin with steep continental slopes or *vice versa* an anticyclonic flow around a mountain range; in this context, the outcome of topographic turbulence is referred to as the *Neptune effect* (Holloway, 1992).

In summary, we learn from topographic turbulence that strong pattern correlations are likely to develop between the streamfunction and the topography, in association with reduced cascade, mixing, and dissipation rates.

6 3D Geostrophic Turbulence and Coherent Vortices

If both f and N are spatially uniform (*i.e.,* in an approximation in which L and H, respectively, are small compared to the scales of variation of these environmental influences), we can transform to a "stretched" vertical coordinate, $z' = Nz/f$, and re-write the QG equations, ((2), ((3), and ((8), in the following form:

$$\begin{aligned} \frac{\partial q}{\partial t} + J(\psi,\, q) &= n.c.t.\,, \quad \text{where} \\ q \;=\; \left[\nabla_h^2 + \frac{\partial^2}{\partial z'^2}\right]\psi &= \nabla'^2\psi\,. \end{aligned} \tag{31}$$

(Note that $R_d' = H$ in this stretched coordinate system.) Thus, the $q[\psi]$ relation is fully isotropic and homogeneous in 3D, although the advective operator remains isotropic and homogeneous only in 2D. As a result we can write the inviscid quadratic invariants as

$$E \;=\; \int\int\int d\mathbf{x}'\; \frac{1}{2}(\nabla'\psi)^2, \quad Z \;=\; \int\int\int d\mathbf{x}'\; \frac{1}{2}(\nabla'^2\psi)^2\,, \tag{32}$$

which are 3D-symmetric relations. In E the term $\propto \psi_{z'}^2$ is the potential energy, and in q, hence Z, the term $\propto \psi_{z'z'}$ is the *vortex stretching* component that combines with the relative vorticity, $\nabla_h^2\psi$, in the Lagrangian parcel invariant q. Thus, except for the presence of ∇', rather than ∇_h, ((31)-((32) are isomorphic to the equations of homogeneous 2D turbulence, away from all boundaries.

This led Charney (1971) to conjecture that there exist 3D stretched-isotropic inverse and forward cascades of E and Z in geostrophic turbulence, with inertial range forms analogous to those in 2D but for the generalization of $\mathbf{k}_h\ (2D) \;\rightarrow\; \mathbf{k}'\ (3D)$. Note that the isotropy here refers to the spatial scale content of q and ψ, not to the velocity field, which remains anisotropic, with

$$w \;=\; -\,\frac{f}{N^2}\frac{D}{Dt_g}\frac{\partial\psi}{\partial z'} \tag{33}$$

smaller by $\mathcal{O}(Ro)$ than

$$\mathbf{u}_h \;=\; \hat{\mathbf{z}} \times \nabla_h\psi\,. \tag{34}$$

This conjecture is supported by the occurrence of k_h^{-3} shapes for the $\mathbf{u}_h$ and T wavenumber spectra in the synoptic range in the atmospheric troposphere and k_h^{-5} shape for geopotential height

in the mesoscale range in the upper ocean (see the figures in *2D Homogeneous Turbulence*). This conjecture also implies an *energy equipartition* such that the potential energy in ((32) is half the kinetic energy, both for the total energy and as a function of wavenumber throughout the inertial ranges. The Charney conjecture clearly must fail at the larger scales, where the finite depths of the ocean or troposphere and lateral non-uniformities in the domains break the isotropy and homogeneity symmetries, where the spatial variations in $f(y)$ and $N(z)$ are important, and where anisotropic, inhomogeneous planetary-scale mean circulations occur, but it is a plausible and important idealization for the advective dynamics on the smaller scales of geostrophic currents and winds. In particular, the Charney conjecture does not apply to the barotropic mode, which may be viewed as occurring on an infinite vertical scale (or, more practically, on the vertical scale of the domain); the barotropic mode often has substantial energy in the ocean and atmosphere, and it does not satisfy the 3D stretched-isotropy symmetry since there is no physically meaningful component of the flow with the form $(\psi(z',t),\ q(z',t))$ that is distinct from the mean stratification. Nevertheless, from random initial conditions or forcing on the indicated small scales, a regime of homogeneous geostrophic turbulence may ensue until such time as the inverse energy cascade brings these larger-scale influences into play.

A numerical study of this regime is made analogous to earlier studies of decaying 2D turbulence), with isotropic, homogeneous, random, narrow-band initial conditions in a triply periodic cubic domain in $\mathbf{x}'$ (McWilliams *et al.*, 1994). The evolution shows approximate conservation of E, dissipation of Z after several eddy turn-over times, and growth of intermittency in the potential vorticity field due to the emergence of coherent vortices (Fig. 9).

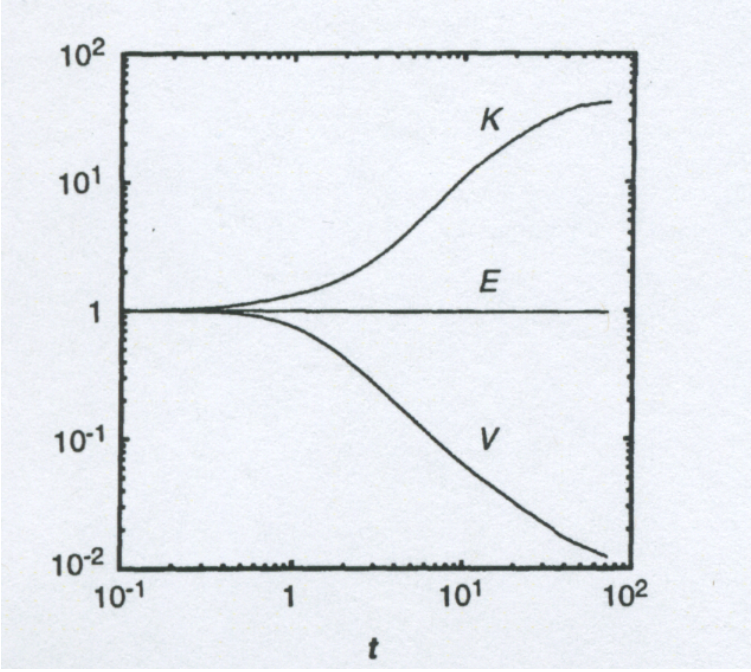

Figure 9: Time series of the energy E, potential enstrophy $V\ (= Z)$, and potential-vorticity kurtosis K in freely evolving 3D geostrophic turbulence. All quantities are normalized by their initial values. These show the cascade tendencies of energy conservation, enstrophy dissipation, and intermittency growth. (McWilliams *et al.*, 1994)

We define the potential enstrophy spectrum as a function of the 3D stretched-isotropic wavenumber $\kappa = (k_x^2 + k_y^2 + k_{z'}^2)^{1/2}$ as

$$S(\kappa) \;=\; \int\int\int_{|\mathbf{k}|=\kappa} |\hat{q}(\mathbf{k})|^2 \, d\mathbf{k} \,, \tag{35}$$

where the caret denotes Fourier transform. The enstrophy spectrum shape at a time close to the peak enstrophy dissipation rate is approximately the forward cascade shape κ^{-1}, although it later steepens after the coherent vortices come to dominate the evolution (Fig. 10).

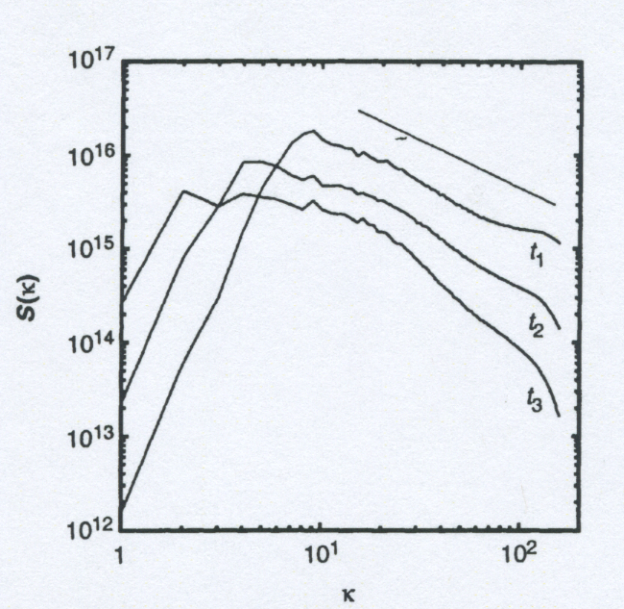

Figure 10: Isotropic wavenumber spectra of potential vorticity $S(\kappa)$ in freely evolving 3D geostrophic turbulence at non-dimensional times of $t_1 = 2$, $t_2 = 5$, and $t_3 = 10$. The interval from the spectrum peak to $\kappa \approx 1000$ is the inertial range (with the comparison line $\propto \kappa^{-1}$), and the dissipation range is for $\kappa > 100$. (McWilliams *et al.*, 1994)

We can test the Charney stretched-isotropy hypothesis by forming the measure,

$$A(\kappa) \;=\; \frac{3T_{z'}}{T_x + T_y + T_{z'}} \,, \tag{36}$$

where the components are quadratic wavenumber weights of the potential enstrophy spectrum:

$$T_i(\kappa) \;=\; \int\int\int_{|\mathbf{k}|=\kappa} \left(\frac{k_i}{\kappa}\right)^2 |\hat{q}(\mathbf{k})|^2 \, d\mathbf{k} \tag{37}$$

for $i = x,\ y,\ z'$. If the flow were stretched-isotropic, then A would equal one for all wavenumbers; alternatively, $A(\kappa) > 1$ (or < 1) implies that the associated structures at wavenumber κ have smaller (or larger) vertical size compared to its horizontal size. In the freely decaying QG turbulence problem, the Charney hypothesis is approximately confirmed by A being not too far from (Fig. 11) unity. However, there are clear departures of different types in the dissipation range

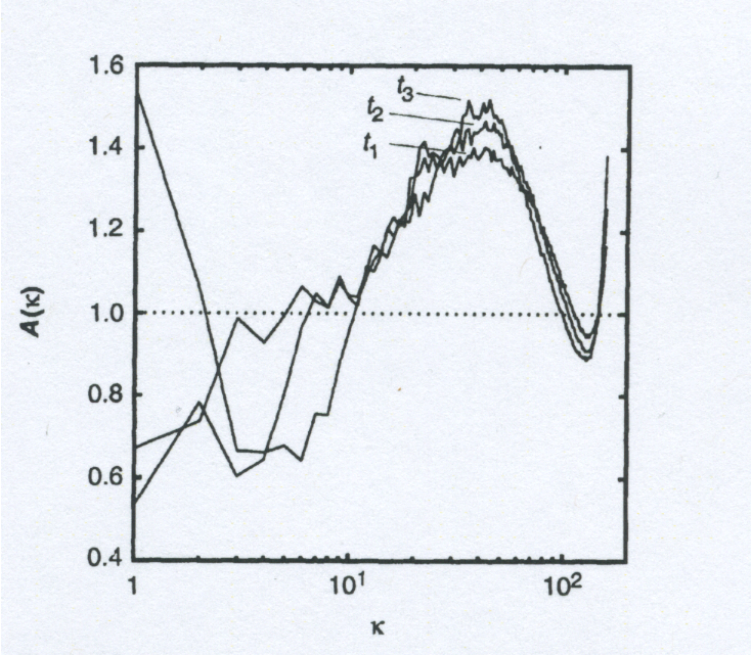

Figure 11: Spectrum anisotropy measure $A(\kappa)$ at the same times as in Fig. 10. A value of $A(\kappa) \neq 1$ indicates an anisotropic potential vorticity distribution at wavenumber κ, and $A < 1$ indicates "short, fat" structures relative to $H/L = f/N$. (McWilliams *et al.*, 1994)

(with $A > 1$), in the enstrophy cascade range (with $A > 1$ due to coherent vortices that have an aspect ratio $H'/L \approx 0.8$ on average), and in the energy containing range (with $A < 1$ because the barotropic component is appreciable).

The coherent vortices are 3D monopoles in q, with an aspect ratio slightly less than 1, with an associated axisymmetric azimuthal velocity field (Fig. 12). They move by chaotic mutual advection in a usually conservative way, but have intermittent close approaches with strong, dissipative interactions. The most important of these are *merger* (as in 2D) and *alignment* (where nearby but vertically displaced, like-sign potential vorticity distributions evolve with only modest dissipation toward having their q extrema on a common vertical axis). These interactions lead to a vortex population with fewer, larger, sparser vortices. At late time, after all possible merger and alignment interactions have occurred, a non-turbulent end-state is reached, consisting of two, opposite-sign, fragmented columns of the surviving elemental vortices. In this end-state the barotropic energy fraction is quite large, although the enstrophy fraction is much smaller.

An important question in 3D geostrophic turbulence is the role of bottom drag as an energy sink. For flows with an inverse energy cascade in a domain with finite depth, the energy transfer has to become primarily into the barotropic mode — often called *barotropization* — once the energy spectrum peak scale is as large as the largest baroclinic deformation radius (Salmon, 1982). There is a current debate about how far and fast barotropization proceeds; the solution featured in this section has an inhibition for barotropic energy transfer due to the coherent 3D vortices, although still the barotropic energy fraction increases with time. Barotropic flows will have a significant bottom velocity, hence be susceptible to bottom drag. Arbic and Flierl (2004) show that the drag coefficient has an important influence on the quasi-equilibrium eddy spectrum. Bottom

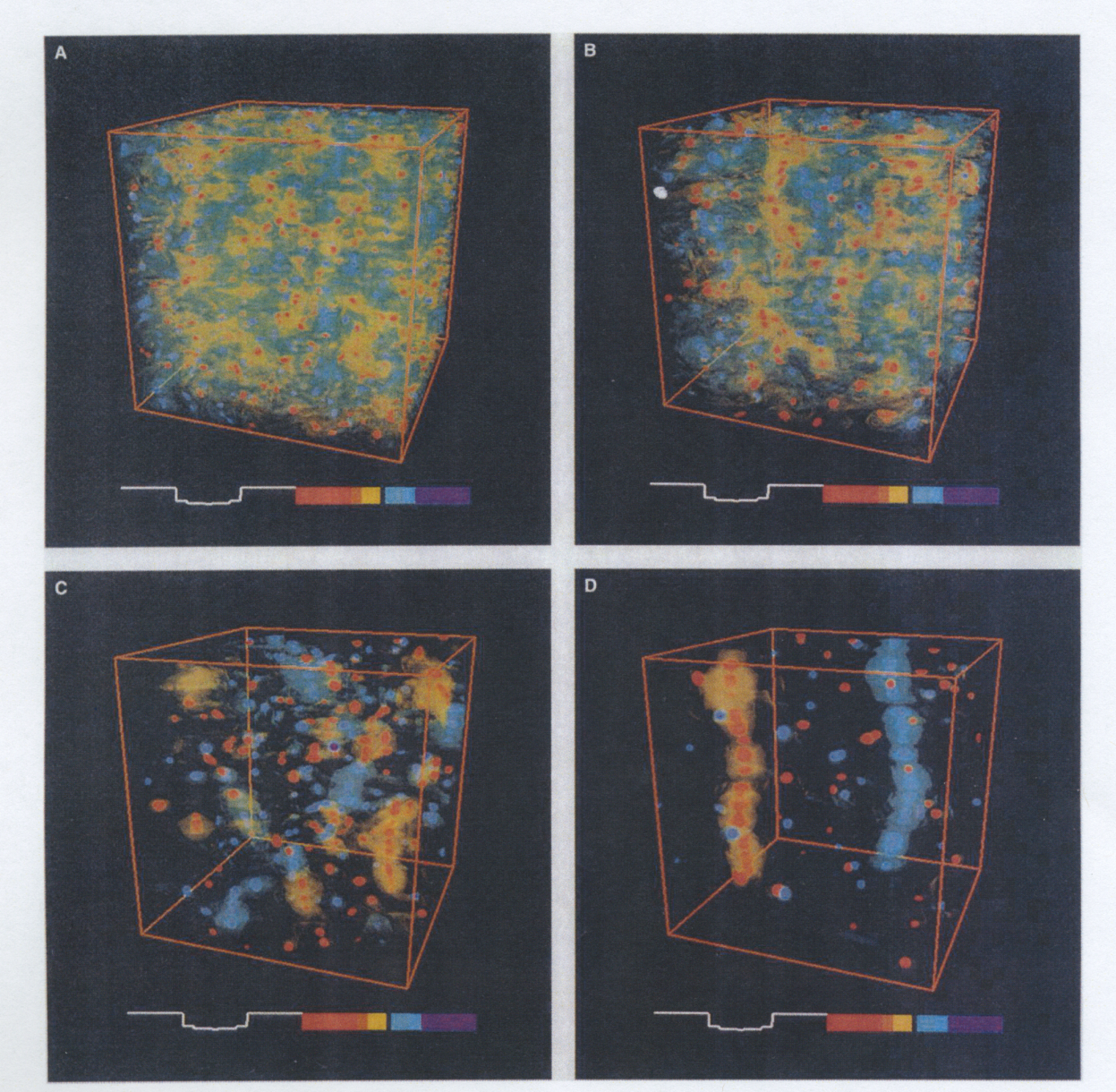

Figure 12: Visualization of the potential vorticity field in 3D QG turbulence at successive times. Elemental coherent structures are 3D monopoles in q, and at late time they aggregate in columns consistent with increasingly barotropic flow. (McWilliams *et al.*, 1994)

drag is also potentially important in an equilibrium zonal jet (Sec. 7), and by some estimates it may be an important competitor with submesoscale breakdown of geostrophic balance in the oceanic energy balance (Sen *et al.*, 2008; see Sec. 9).

In summary, we learn from 3D geostrophic turbulence that many of the distinctive evolutionary behaviors found in the unphysical model of 2D turbulence — and, by extension, in the 2D generalizations of β, γ, and topographic turbulence- – also have relevance in the real 3D world.

7 A Baroclinic Zonal Jet

Geophysical turbulence of all types contributes to the maintenance of the general circulation in the ocean and atmosphere, since the external forcings (*i.e.,* the sources) occur on the planetary scale; the actual mixing and dissipation (*i.e.,* the sinks) occur on the molecular kinetic scale, as represented in fluid dynamics through viscosity and diffusion; and the turbulent cascades that connect these large and small scales must pass through all the regimes we have discussed in these lectures. Here I will focus only on the geostrophic turbulence contribution at mesoscales and larger. Moreover, for simplicity, I will consider only a highly idealized — but perhaps most fundamental and famous — GFD problem of a forced zonal jet that is x-symmetric and t-stationary and wider in y than its largest baroclinic deformation radius, $L > R_d$. This is qualitatively similar to the mid-latitude atmospheric westerlies (forced by meridional heating differences) and the oceanic Antarctic Circumpolar Current (ACC) (forced by an eastward surface wind stress). We will make the QG, β-plane, and small-amplitude topography approximations. To further focus on the roles played by geostrophic turbulence, we assume that the fluid is quasi-adiabatic (*i.e.,* with no material mixing or advection across the stably stratified isopycnal surfaces), so that the external forcing influences of heating and stress are merely imposed without explicitly including the small-scale turbulence (*e.g.,* in the PBL) generally associated with their occurrence.

Because this problem is given a detailed treatment in Sec. 5.3 in McWilliams (2006) — which is substantially based on McWilliams and Chow (1981) and a similar study by Wolff *et al.*(1991), and consistent with a more modern study by Roullet *et al.* (2011) — here I will only summarize the primary phenomena and interpretations without showing many figures. The purpose is to demonstrate the conceptual framework and language for how turbulence shapes the general circulation.

To be specific we will focus on the wind-driven version of this problem with an eastward surface stress $W_s^{(}(x))(y) > 0$ in a mid-latitude band in the southern hemisphere ocean with $f(y) < 0$ (*i.e.,* an idealized ACC). To localize the jet we assume that $\tau_s^{(}(x))$ is zero outside of a central meridional region. The fluid is stably stratified with background buoyancy frequency $N(z)$, and we assume the temperature evolution is adiabatic.

After an initial spin up from a stratified resting state, the mean zonal flow $\overline{u}(y,z)$ generates geostrophic turbulence from a primarily baroclinic instability. In equilibrium the mean jet is surface intensified at the latitude of the maximum wind stress, and the associated geostrophic, hydrostatic temperature $\overline{T}(y,z)$ is colder on the polar side.

$$.\overline{u} \;=\; -\frac{1}{f}\partial_y\overline{\phi} \qquad \partial_z\overline{\phi} \;=\; \alpha g\overline{T}\,. \tag{38}$$

α is the thermal expansion coefficient. We define a mean geostrophic streamfunction by $\overline{\psi} = \overline{\phi}/f$. A sketch of this mean jet configuration is in Fig. 13. The mean circulation is $(\overline{u},\overline{v},\overline{w})$, where

only the zonal component is in geostrophic balance since $\partial_x \overline{\phi} = 0$ by the zonal symmetry (or periodicity). The mean-flow components in the meridional plane are thus ageostrophic velocities, weaker by $\mathcal{O}(Ro)$.

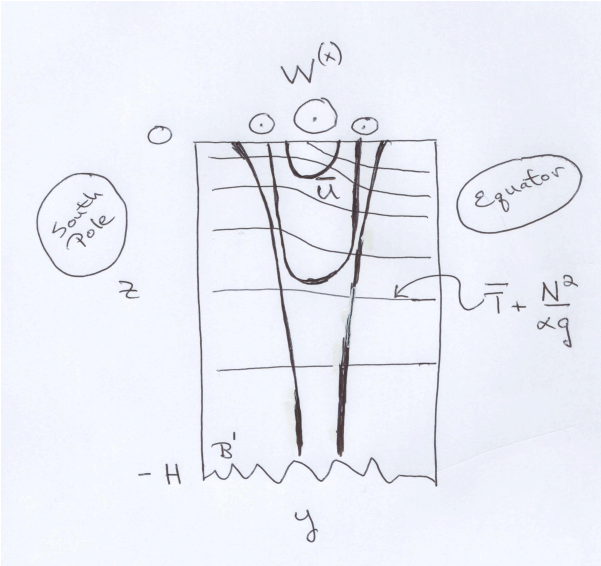

Figure 13: Sketch of the mean zonal flow $\overline{u}(y,z)$ and temperature structure $\overline{T}(y,z) + N^2(z)/(\alpha g)$ in an idealized equilibrium zonal jet. The surface wind stress $W_s^{(x)}(y)$ and bottom topographic variation $B'(x,y)$ are also indicated.

Now consider the fully developed, statistical equilibrium state. The flow field is illustrated in Fig. 14. A central dynamical balance is for the mean zonal momentum:

$$\partial_t \overline{u} \;=\; 0 \;=\; -\,\partial_z \tau^{(x)} - \;\partial_y R^{(x)} + n.c.t. \tag{39}$$

The most important part of this balance for a wide jet with weak interior diffusion (*i.e.,* the non-conservative term $n.c.t.$) is associated with the flux of zonal momentum $\tau^{(x)}$ downwards from the surface where the eastward stress is applied down to the bottom where a balancing westward drag force occurs.

$$\begin{aligned} \tau^{(x)} &= -W_s^{(x)}\,, \qquad z \;=\; 0 \\ &= -\,D^{(x)}\,, \qquad -H < z < 0 \\ &= -\left[D_b^{(x)} + \epsilon_b \overline{u}_b\right], \qquad z \;=\; -\,H\,. \end{aligned} \tag{40}$$

(The sign conventions here are historical, consistent with W_s being the stress of the wind on the ocean and τ being the upward momentum flux.) $D^{(x)} = -f\overline{v'\eta'}$ is the isopycnal-surface or interfacial form stress associated with the geostrophic eddies (with $\eta = -\alpha g T/N^2$ the interfacial height displacement); $D_b^{(x)} = -f\overline{v_b' B'}$ is the topographic form stress associated with a bottom elevation anomaly $B'(x,y)$ and bottom velocity v_b'. ϵ_b [m s^{-1}] is a bottom drag coefficient associated with a bottom Ekman layer. It doesn't take very much amplitude in the topography for D_b to be the dominant bottom stress (Treguier and McWilliams, 1990), although ϵ_b remains an important parameter for energy dissipation (where bottom form stress does not contribute). The remaining

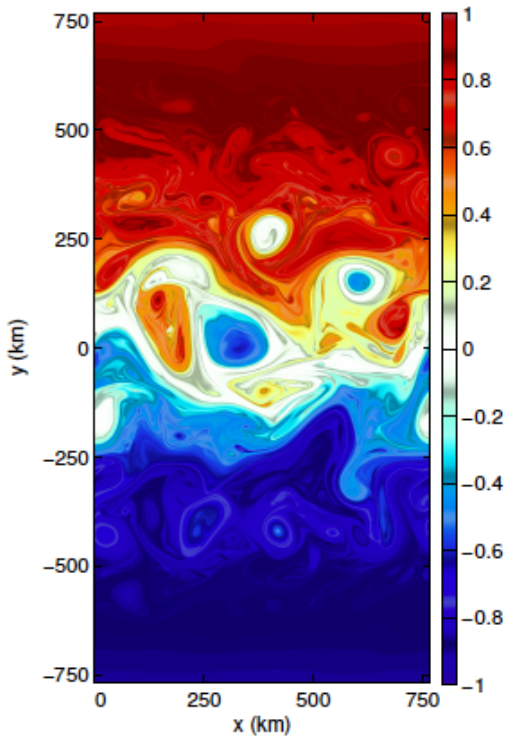

Figure 14: Snapshot of the potential vorticity $q(x, y)$ near the top surface in a statistical equilibrium turbulent regime for a baroclinic zonal jet (in a northern hemisphere domain with $\partial_y \overline{b} > 0$ and $\partial_y \overline{q} > 0$). The geostrophic eddies arise primarily by baroclinic instability of the mean jet $\overline{u}(y, z)$, and eddy fluxes equilibrate it against the mean forcing. (Roullet *et al.*, 2011)

term in (39) is the horizontal eddy Reynolds stress divergence with $R^{(x)} = \overline{u'v'}$. In a full-depth and cross-jet integral the balance is

$$\frac{\partial}{\partial t} \int_{-H}^{0} \int_{-\infty}^{\infty} \overline{u}\, dz\, dy \;=\; 0 \;=\; \int_{-\infty}^{\infty} \left[W_s^{(x)} - D_b^{(x)} - \epsilon_b \overline{u}_b \right] dy\,, \tag{41}$$

ignoring $n.c.t.$ and noting that $R^{(x)} \to 0$ as $y \to \pm\infty$ due to far-field dissipation of fluctuations or meridional boundaries. This shows that the surface and bottom stresses balance each other in an integral sense, while the interior eddy momentum fluxes $D^{(x)}$ and $R^{(x)}$ respectively act only to redistribute mean zonal momentum vertically and horizontally.

Figure 15 sketches the shapes of $D^{(x)}$ and $R^{(x)}$. The form stress mirrors the surface stress, and the Reynolds stress is essentially counter-gradient by acting to accelerate the jet core and decelerate its edges. The cause of this behavior in $R^{(x)}$ is meridional Rossby wave radiation away from the jet center where the eddies are most strongly generated (see the remark at the end of Sec. 4 and Chap. 5.4, McWilliams, 2006, for a full analysis). When the meridional scale of the wind stress is much larger than $L_\beta > R_d$, multiple jets can occur, with a meridional scale near L_β (Panetta, 1993; Treguier and Panetta, 1994); the reasons for this are similar to the dynamics of β turbulence discussed above.

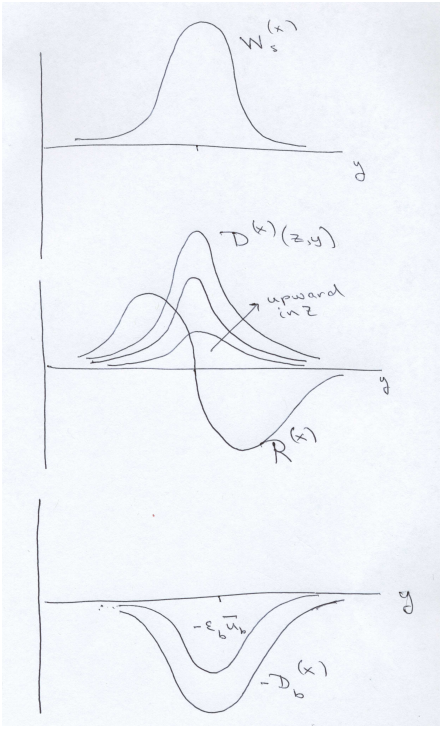

Figure 15: Sketch of the principal terms in the mean zonal momentum balance (39) for an idealized equilibrium zonal jet.

Now consider the ageostrophic secondary circulation in the meridional plane. The kinematic relation expressing the movement of the interfaces as material surfaces is

$$w \;=\; \frac{D\eta}{Dt}\,. \tag{42}$$

The mean of this relation is

$$\overline{w} \;=\; \partial_y \overline{v'\eta'} \;=\; -\frac{1}{f}\,\partial_y D^{(x)}\,. \tag{43}$$

Given the shape of $D^{(x)}$ this implies a downward flow on the equatorial side of the jet and upward flow on the polar side. By the mean continuity balance in the interior,

$$\partial_y \overline{v} + \partial_z \overline{w}_z \;=\; 0, \;\; \text{or} \tag{44}$$

$$\overline{v} \;=\; \frac{1}{f}\,\partial_z D^{(x)}\,. \tag{45}$$

We combine (43) and (45) with the approximation that the surface PBL lies entirely within the upper layer of the model configuration, *i.e.,*

$$\overline{w} \;=\; w_{ekman} \;=\; -\frac{1}{f}\partial_y W_s^{(x)} \;\text{ at }\; z=0\,, \tag{46}$$

and there is a surface, equatorward mean Ekman-layer transport,

$$\overline{v} \;=\; v_{ekman} \;=\; -\frac{1}{f}\,W_s^{(x)} > 0 \;\text{ at }\; z=0\,. \tag{47}$$

Thus we obtain the clockwise mean meridional circulation seen in Fig. 16. This mean meridional overturning circulation is called the Deacon Cell in the ACC and the Ferrel Cell in the atmospheric Westerlies (sinking motion on the equatorial side, rising on the poleward, *i.e.,* a "thermally indirect" circulation, which is different from the diabatic "thermally direct" tropical atmospheric Hadley circulation driven by equatorial convection). By our present analysis we can see that it is "eddy driven" in the sense that it is dynamically balanced by the interior geostrophic eddy flux D. In a less adiabatic model, other micro-scale turbulent mixing effects, or in the case of Earth's atmosphere interior diabatic heating and cooling, enter these relations and interfere with the simple adiabatic balance of $\overline{\mathbf{u}} + \mathbf{u}^* = 0$.

A mean heat balance, at leading order, has the form,

$$\partial_t \overline{T} \;=\; 0 \;=\; -\,\partial_y \overline{v'T'} - \frac{N^2}{\alpha g}\overline{w}\,, \tag{48}$$

where the eddy heat flux is related to the eddy form stress by

$$\overline{v'T'} \;=\; \frac{N^2}{\alpha g f}\,D^{(x)}\,. \tag{49}$$

Thus, positive form stress is associated with poleward heat flux. The down-gradient eddy heat flux here (*i.e.,* opposite in sign to $\partial_y \overline{T} > 0$) is a signature of eddy generation by baroclinic instability. In (49) the eddy heat flux divergence is balanced by vertical advection of the background stratification by the meridional overturning circulation.

What I have just presented is a picture that was first drawn in the 1950s and 1960s to describe the maintenance of the jet stream (*e.g.,* Lorenz, 1967), even though for many years afterward it was still a serious challenge to realize computational solutions with this behavior. The equilibrium

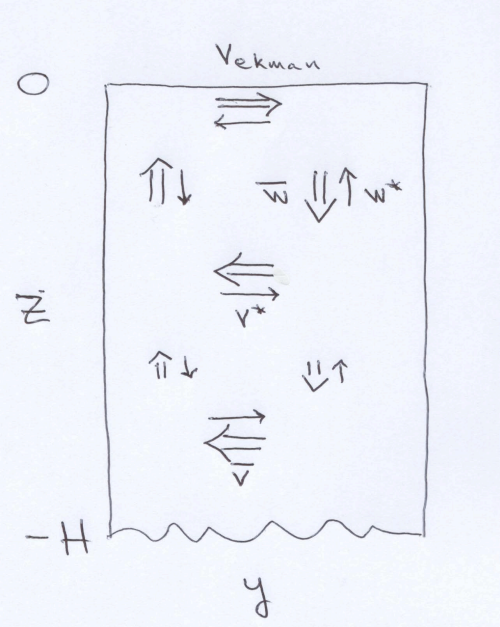

Figure 16: Sketch of the Eulerian mean meridional overturning circulation $(\overline{v}, \overline{w})$ (thick arrows) and the opposing eddy-induced overturning circulation (thin arrows) for an idealized equilibrium turbulent zonal jet.

geostrophic-turbulent jet is such an important GFD problem that it has developed several associated interpretations that I will briefly mention here.

Eulerian Mean Circulation: $(\overline{u}, \overline{v}, \overline{w})$

Eliassen-Palm (EP) flux: $\mathbf{F} = (0, -R, D)$. Notice that the mean, interior, zonal momentum balance (39) can be written as

$$-\nabla \cdot \mathbf{F} = n.c.t.. \tag{50}$$

The dynamical meaning of $\mathbf{F}$ is that it is the eddy forcing of the zonal mean flow (Andrews *et al.*, 1987).

Eddy Potential Vorticity Flux: with the 3D QG definition of q,

$$q = f_0 + \beta y + \partial_x v - \partial_y u - f\partial_z \eta \,, \tag{51}$$

we can write

$$\overline{v'q'} = \partial_z D^{(x)} - \partial_y R^{(x)} = \nabla \cdot \mathbf{F} \,. \tag{52}$$

This is yet another way to characterize the eddy terms in the mean zonal momentum equation.

Residual Mean Circulation: $(\overline{u}, \overline{\widetilde{v}}, \overline{\widetilde{w}})$, where

$$\overline{\widetilde{v}} = \overline{v} - \frac{1}{f}\,\partial_z D^{(x)}, \;\; \overline{\widetilde{w}} = \overline{w} + \frac{1}{f}\,\partial_y D^{(x)} \,. \tag{53}$$

The final r.h.s. terms are the non-divergent *eddy-induced transport velocity*, $\mathbf{u}^*$, that appears in the eddy tracer transport parameterization of Gent and McWilliams (1990), and $(\overline{\widetilde{v}}, \overline{\widetilde{w}})$ is the relevant total advection velocity in a transformed Eulerian mean model (both below).

Non-acceleration, Non-interaction, and Eliassen-Palm theorems: In equilibrium and with $n.c.t. = 0$, there is no driving of the zonal mean flow by the turbulent eddies.

Eddy Advection and Isopycnal Mixing: The eddy-induced velocity is non-divergent, which implies that it can be expressed in terms of a vector streamfunction,

$$\mathbf{u}^* \;=\; \nabla \times \mathbf{\Psi}^* \,. \tag{54}$$

For a jet with zonal symmetry, $\mathbf{\Psi}^* = \hat{\mathbf{x}} \Psi^{*(x)}$, and $v^* = \partial_z \Psi^{*(x)}$, $w^* = -\partial_y \Psi^{*(x)}$. The fundamental definition of $\mathbf{\Psi}^*$ is in terms of the so-called skew component of the eddy buoyancy flux (rather than the component in the direction of the mean buoyancy gradient $\nabla \overline{b}$); *i.e.,*

$$\mathbf{\Psi}^* \;=\; -\, \frac{\overline{\mathbf{u}' b'} \times \nabla \overline{b}}{|\nabla \overline{b}|^2} \tag{55}$$

(Ferrari *et al.*, 2008). With this definition and (54),

$$\nabla \cdot \overline{\mathbf{u}' b'} \;=\; \mathbf{u}^* \cdot \nabla \overline{b} \,; \tag{56}$$

i.e., the eddy flux divergence has the form an addition advection of mean buoyancy by the eddy-induced velocity $\mathbf{u}^*$. (The other component of the eddy flux, parallel to $\nabla \overline{b}$, leads to an eddy-diffusion type of term in the mean buoyancy balance equation which by definition is oriented along the mean isopycnal surfaces.) For a jet with zonal symmetry, $b = \alpha g T$, and mean vertical stratification dominant in $|\nabla \overline{b}|$,

$$\Psi^{*(x)} \;=\; -\, \frac{\overline{v' b'}}{N^2} \;=\; \frac{1}{f}\, D^{(x)} \,. \tag{57}$$

Hence,

$$v^* \;=\; -\, \frac{1}{f}\, \partial_z D^{(x)} \,, \qquad w^* \;=\; \frac{1}{f}\, \partial_y D^{(x)} \,. \tag{58}$$

Thus, the eddy-induced velocity is equal and opposite to the Eulerian mean meridional overturning circulation $(\overline{v}, \overline{w})$, and the residual circulation $(\widetilde{\overline{v}}, \widetilde{\overline{w}})$ is zero in an adiabatic flow (Fig. 16). So the apparent material advection by the Deacon or Ferrel Cells is illusory since it is canceled by the eddy-induced advection. If the fluid is truly adiabatic, then this cancellation is necessary to avoid mean Lagrangian trajectories crossing mean isopycnal surfaces. Of course, if there are diabatic processes (as near the oceanic surface or in the troposphere), this cancellation will be partially incomplete.

Eddy Parameterization: The preceding relations are a diagnostic characterization for the eddy buoyancy flux, under the presumption that measurements or turbulent solutions are available for analysis. However, in models that do not resolve their eddies, either not at all or only partially, then the missing eddy fluxes must be parameterized. Within a framework proposed by Gent and McWilliams (1990), the parameterized evolution equation for the large-scale tracer field, c, is

$$\frac{Dc}{Dt} \;=\; -\mathbf{u}^* \cdot \nabla c + \mathcal{R}[c] \,, \tag{59}$$

where $\mathcal{R}$ is an isopycnally-oriented diffusion operator that mixes tracers along isopycnal surfaces but not across them (and thus has no effect on b itself). Note that we could alternatively write the

advection operators in (59) using only $\tilde{\mathbf{u}}$ as if it were the total Lagrangian mean velocity (*cf.,* the role of Stokes drift in the wave-averaged Langmuir PBL model). An eddy-diffusion hypothesis in (55) — *i.e.,* down-gradient eddy mass flux within isopycnal layers — leads after some rather complex manipulations to the parameterization formula,

$$\mathbf{\Psi}^* \ = \ -\kappa_{GM} \, \frac{\hat{\mathbf{z}} \times \nabla b}{\partial_z b} \, , \tag{60}$$

or for the mean symmetric QG jet,

$$\mathbf{\Psi}^{*(x)} \ = \ \kappa_{GM} \, \frac{\partial_y b}{\partial_z b} \ = \ \alpha g \kappa_{GM} \, \frac{\partial_y \overline{T}}{N^2} \, . \tag{61}$$

$\kappa_{GM} > 0$ is an eddy diffusivity. The parameterization principle is down-gradient eddy diffusion of mean horizontal buoyancy gradient (or, more precisely in a generalization beyond QG, down-gradient mixing of mean isopycnal layer thickness, which leads to an integral loss of mean available potential energy through an implied eddy generation by baroclinic instability). This parameterization has been found to give more realistic solutions in oceanic GCMs, compared to its historical alternative of horizontal eddy diffusion of tracers, and at present it is used in almost all OGCM calculations in which the mesoscale eddies are not resolved (*i.e.,* the horizontal grid scale is $\mathcal{O}(100)$ km or larger). Most calculations of the ocean circulation for climate studies use such a coarse resolution, simply as a necessity of computational economics.

Transformed Eulerian Mean Equations (Andrews *et al.*, 1987; Plumb and Ferrari, 2005): Since $\mathbf{u}^*$ acts as an extra advection velocity for material tracers and tends to cancel $\overline{\mathbf{u}}$ advection in nearly adiabatic equilibrium, there is a theoretically attractive compactness to writing an eddy-averaged model in terms of the residual mean velocity $(\overline{u}, \overline{\tilde{v}}, \overline{\tilde{w}})$.

In summary, we learn from geostrophic turbulence how "geostrophic eddies" play essential roles in maintaining the planetary-scale circulations through their horizontal Reynolds stress, isopycnal form stress, topographic form stress, and lateral buoyancy flux.

8 Surface Quasigeostrophic (SQG) Turbulence

A strongly simplified GFD model assumes the QG approximation with a few twists: the interior stratification is uniform (*i.e.,* constant N), f is constant ($\beta = 0$), the QG potential vorticity (8) is zero, but there is a non-trivial surface temperature, $(\alpha g/f)T = \theta(x, y, t) = \partial_z \psi(x, y, 0, t)$. The surface buoyancy equation is

$$\frac{D}{Dt_g} \theta \ = \ n.c.t. \ \text{ at } \ z = 0 \tag{62}$$

since there $w = 0$. $\psi(x, y, z, t)$ is determined throughout the volume by inverting a homogeneous 3D Poisson equation (since $q = 0$),

$$\left(\nabla_h^2 + \frac{f^2}{N^2} \partial_{zz} \right) \psi \ = \ 0 \, , \tag{63}$$

with an inhomogeneous Neumann boundary condition,

$$\partial_z \psi \ = \ \theta \ \text{ at } \ z = 0 \, . \tag{64}$$

This system has two non-trivial quadratic conservative invariants (when $n.c.t. = 0$). One is the familiar volume integrated energy, E in (12), and the other is surface temperature variance (here rescaled as a QG surface available potential energy density $\mathcal{A}_s$),

$$\mathcal{A}_s \;=\; \frac{f^2}{2N^2} \int\int dx\, dy\, \theta^2 \,, \tag{65}$$

which is just a rescaled version of the surface temperature spectrum, $E_{\theta s}$. The usual second quadratic invariant for QG, the potential enstrophy, is trivial for the SQG model since $q = 0$.

From (62)-(63) and the QG momentum equation at $z = 0$ after subtracting out geostrophic balance,

$$\partial_t \mathbf{u}_{gs} = -\,(\mathbf{u}_{gs} \cdot \nabla_h)\mathbf{u}_{gs} - \; f\hat{\mathbf{z}} \times \mathbf{u}_{as} + n.c.t. \tag{66}$$

(where the subscript s refers to the upper surface and the subscripts g and a to geostrophic and ageostrophic velocity components, respectively), we Fourier transform in horizontal wavenumber and derive the evolution equations for surface kinetic energy and density variance spectra in wavenumber space:

$$\begin{aligned} \partial_t E_{ugs} &= \Pi_u + \Pi_a + n.c.t. \\ \partial_t E_{\theta s} &= \Pi_\theta + n.c.t.\,. \end{aligned} \tag{67}$$

Apart from the n.c.t., the right-side terms are the wavenumber spectrum transfer functions associated, respectively, with geostrophic momentum advection, ageostrophic Coriolis force, and geostrophic temperature advection, all derived from the surface momentum and temperature equations above. Π_a, in particular, represents a pressure work associated with the ageostrophic horizontal divergence (*i.e.,* $\partial_z w$) and the surface pressure.

Blumen (1978) worked out the inertial cascade ranges for SQG, which differ from the Charney (1971) ranges because of the different quadratic invariants. Again, there are two such ranges: a forward cascade range for E_{θ_s} with its horizontal wavenumber spectrum $\propto\; k^{-5/3}$ (which is equivalent to the shape of the surface kinetic energy spectrum, $E_{u_{gs}}(k)$), and an inverse energy cascade range for the depth-integrated total geostrophic energy, accompanied by a $E_{u_{gs}} \sim E_{\theta_s}$ whose spectrum is a flatter shape $\propto\; k^{-1}$.

This model has attracted a lot of interest among meteorologists and oceanographers for several reasons:

- A two-boundary form of the SQG model with equal and opposite mean temperature gradients $\overline{\theta}(y)$ is the configuration of one of the original baroclinic instability studies (Eady, 1949).

- The forward energy cascade in $E_{\theta s}$ is a conspicuous exception to the usual QG inverse energy cascades (or vanishing forward energy flux in the enstrophy cascade ranges). However, Hoyer and Sadourney (1982) show that E_{ugs} still has a mostly inverse cascade behavior, Π_u (though not an exact inertial range) in SQG even in the forward $E_{\theta s}$ inertial range, and Capet *et al.* (2008a) show that the forward $E_{\theta s}$ cascade is accompanied by a conversion into surface kinetic energy,

  $$E_{ugs} \;=\; \frac{1}{2} \int\int dx\, dy\, \mathbf{u}_g^2(x, y, 0)\,, \tag{68}$$

  that has the same $k^{-5/3}$ energy spectrum shape and is undergoing an inverse energy cascade that is opposite to the forward $E_{\theta s}$ cascade. Thus, the SQG model does have a partial forward

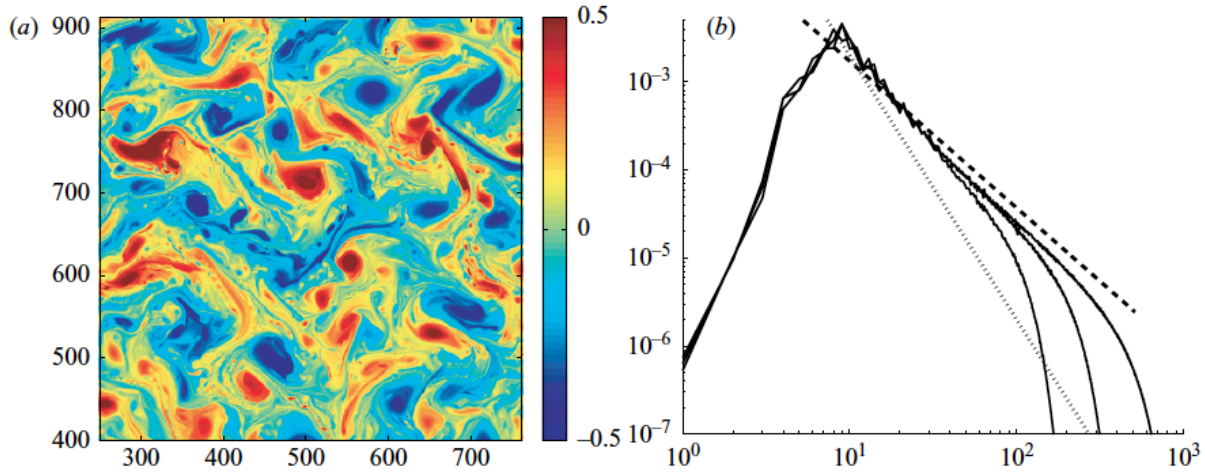

Figure 17: (a) Snapshot of surface density θ in a freely decaying solution for SQG in a horizontally periodic domain with $N = 1024$ grid points in each direction. (b) Isotropic surface horizontal kinetic energy spectrum $E_{u_{gs}}(k)$ for three values of $N = 256, 512, 1024$, with comparison power laws with exponents of -3 and $-\frac{5}{3}$. (Capet *et al.*, 2008a)

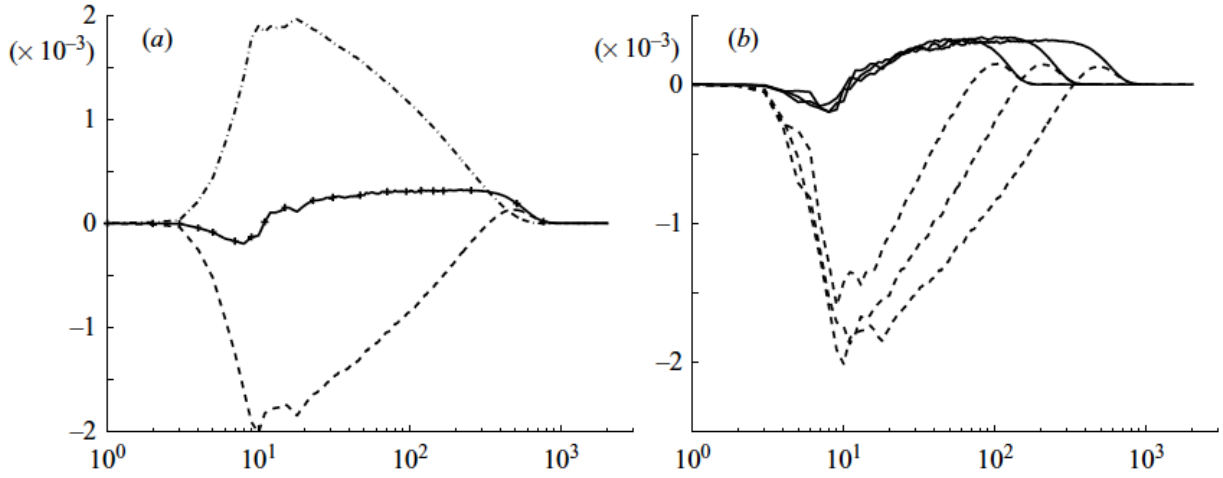

Figure 18: (a) Spectrum transfer functions Π in a freely decaying solution for SQG in a horizontally periodic domain with $N = 1024$ grid points in each direction: for surface temperature variance (Π_θ, solid line), surface kinetic energy due to horizontal geostrophic advection (Π_u, dashed line) and to horizontal ageostrophic advection (Π_a, dot-dashed line). (b) Π_u and Π_ρ for three values of $N = 256, 512, 1024$. (Capet *et al.*, 2008a)

cascade that transfers θ variance toward small scales, but this accomplishes little if any energy dissipation at large Re and does not change the overall inverse-energy cascade behavior of QG dynamics. Freely decaying solutions at large Re that exhibit the approximate forward cascade in $E_{\theta s}(k)$ are shown in Figs. 17-18: in spite of the $\approx\ k^{-5/3}$ spectrum shape and the mostly forward energy cascade shown in $\Pi_\theta > 0$ and active small-scale flow features at the surface, there is an inverse energy cascade in $\Pi_u < 0$ with little net total energy transfer to small-scales and thus with little energy dissipation; ***i.e.,*** surface kinetic energy is supplied by $\Pi_a > 0$ across the whole range of k values, coming from potential energy conversion, and turns the energy around to an inverse cascade to larger scales.

- Another interesting behavior in SQG, related to the preceding one, is that front-like structures develop in θ, so this is a simplest model of surface frontogenesis relevant to atmospheric and oceanic surface fronts. There is even a suggestion, but not a proof, that SQG might form infinite gradients in θ at a finite time (Majda and Tabak, 1996), potentially analogous to the known behavior in a non-QG, "balanced" model called semigeostrophy used for surface fronts (Hoskins and Bretherton, 1972). Nevertheless, the frontogenetic tendency in SQG is rather weak compared what happens in more general hydrostatic or Boussinesq dynamics because of the neglect of ageostrophic temperature advection in (62) (Sec. 9).

Many papers have been written on SQG dynamics (***n.b.,*** Held ***et al.***, 1995; Lapeyre and Klein, 2006), especially in recent years in an oceanic context motivated by submesoscale surface fronts and filaments (but see Sec. 9).

9 Submesoscale Transition and Loss of Balance

As a final brief topic in this section and the next one, consider the dilemmas that geostrophic turbulence theory presents to the general circulation and to smaller-scale turbulence regimes that presume a supply of energy from larger scales to support their forward energy cascades that connect with energy dissipation (***e.g.,*** stratified turbulence). The important energy sources are on very large scale, mainly the time-averaged planetary-scale heating (atmosphere) and surface wind stress (ocean). The mean circulations respond to these forcings but must have compensating energy sinks for climate equilibrium to occur. The principal mean-circulation sink is through geostrophic eddy instabilities. This moves the question to energy sinks for geostrophic turbulence, which are well represented by QG dynamics. But by the results in the rest of this QG chapter, we see that energy is either inverse-cascaded, away from dissipation on small scales, or else it is partly retained on large and intermediate scales if there is forward enstrophy cascade and coherent structures. Recall from the *3D and 2D Homogeneous Turbulence* chapters the inertial range scaling estimates. In the case of a QG forward enstrophy cascade inertial range, the energy spectrum varies as $E(k) \sim V_L^2/L$, with $k = 1/L$. $E \sim k^{-3}$ implies $V_L \sim L$. Thus, the energy cascade rate, $V_L^3/L \sim L^2$; ***i.e.,*** it is vanishing small as L decreases. Furthermore, a scale-local Rossby number in this spectral range is $Ro_L = V_L/fL \sim L^0$, so the Rossby number is constant with scale. If an outer-scale Ro value is small, as is usual for large-scale flows, then by QG dynamics it will remain small down to arbitrary small scales, meaning that the QG assumption of small Ro is self-consistently sustained throughout its forward enstrophy cascade, and there does not need to be any transition to a different type of turbulent dynamics at any scale.

However, even if QG theory has turbulent solutions that are self-consistent at arbitrarily small scales doesn't mean that they are physically valid. Consider several possibilities:

- The shallower $k_h^{-5/3}$ energy spectrum in SQG solutions implies that a scale-local Rossby number is in fact increasing with k_h. This means that that SQG is not self-consistent at small scales, hence that its lack of a net forward energy cascade is unlikely to be correct, hence that energy will forward cascade into non-geostrophic types of turbulence, at least near vertical boundaries.

- Within the asymptotic derivation of QG theory, the vertical velocity can be calculated diagnostically from the geostrophic streamfunction using adiabatic buoyancy balance:

$$w = -\frac{f}{N^2}\frac{D}{Dt}_g \partial_z \psi \,. \tag{69}$$

  This relation can be used to estimate the 3D wavenumber spectrum of w in terms of the 3D wavenumber spectrum of ψ. In particular, in a Charney stretched-isotropic forward-enstrophy cascade range with total energy spectrum $\sim k^{-3}$, the w spectrum is less steep than the $\mathbf{u}_g$ spectrum, especially for small vertical scales. This implies that the neglect of ageostrophic velocities in QG theory becomes invalid at small vertical scales (suggested by the extra ∂_z operator in (69)), hence that the absence of forward energy cascade can no longer be justified. This argument applies to interior QG flows even with isothermal boundary conditions (unlike SQG).

- The QG model has barotropic and baroclinic instability modes that are the source of geostrophic turbulence. There is no reason why these need to be the only types of instability at finite values of Ro and Fr that occur in nature. If an ageostrophic instability of geostrophic flow occurs, its evolution need not be constrained to have only inverse energy cascade.

As a question of general turbulence theory, how is enough dissipation achieved for the general circulation? One possible answer is dissipation in planetary boundary layers (PBL), although the large interior regions of the ocean and atmosphere are not adjacent to the PBL. Another possible answer is an induced dissipation by small-scale motions that might act like an eddy viscosity for the geostrophic eddies (*e.g.,* spontaneous emission of inertia-gravity waves), but thus far this process has not been shown to be a very effective route to dissipation for the general circulation, even though such motions do have effective forward energy cascades to dissipate their own energy (see *Stably Stratified Turbulence*). In atmospheric and oceanic GCMs with usually rather coarse grid resolution, there is significant interior dissipation due to their parameterizations of subgrid-scale eddy diffusion, but it has long remained unclear just what process this is supposed to represent.

Recently several computational examples have been produced of mesoscale flows that spontaneously break their geostrophic, hydrostatic momentum balances on their smaller resolved scales (sometimes referred to as the submesoscale regime). This can occur through frontogenesis and secondary instabilities of geostrophic currents, and when it happens it is accompanied by forward energy cascades that feed into smaller scale stratified and shear cascades *en route* to micro-scale dissipation. If further testing proves that this is generic behavior — *i.e.,* that mesoscale flows spontaneously generate a forward energy cascade — then a direct dissipation route is established from

the mean planetary forcing of the general circulation and its primarily geostrophic instabilities and turbulence down to the microscale regimes of stratified and shear turbulence and further down to 3D isotropic cascade and dissipation (Fig. 19). If so, then this would be the turbulent view of the overall system dynamics of Earth's ocean and atmosphere, simplistic of course but nevertheless a coherent conceptual framework.

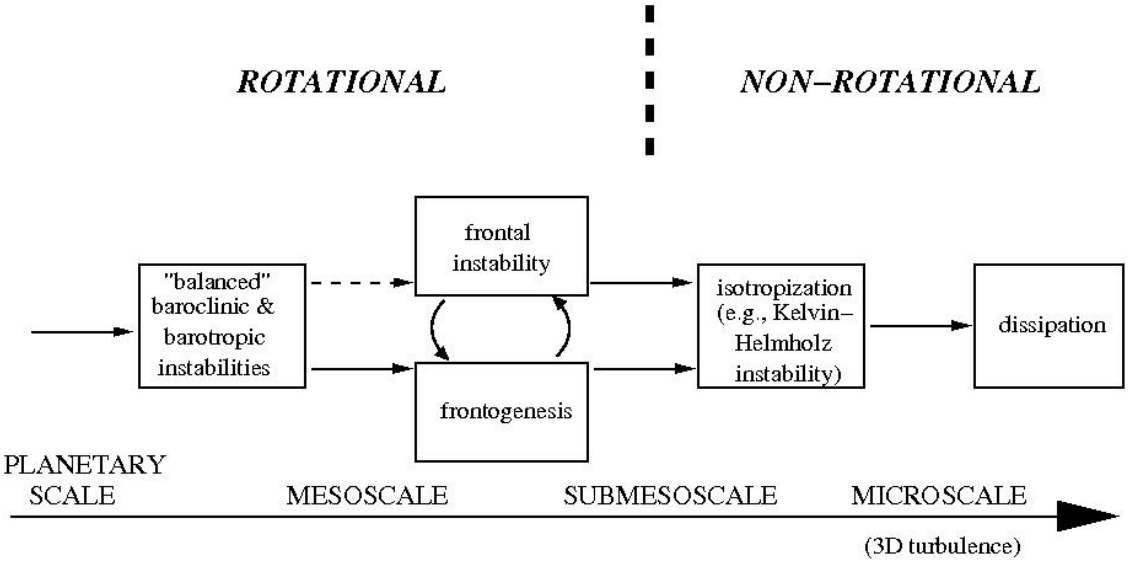

Figure 19: Sketch of the flow of dynamical control and energy from the global forcing of the general circulation through the balanced mesoscale and partially-balanced submesoscale ranges and further through the stratified and shear ranges down to the isotropic microscale where dissipation occurs. (McWilliams, 2010)

Now we examine a small sample of the computational evidence in support of this view of spontaneous submesoscale transition. An idealized turbulence problem has random forcing at relatively large scales (Figs. 20-21). In a rotating, stratified fluid with small Ro and Fr, then develops a forward enstrophy cascade, generally similar to the Charney cascade except for effects of the finite vertical domain size that make the largest scales more like 2D turbulence than 3D. In a succession of cases with higher Ro, the steep shape of the energy spectrum in the enstrophy range develops a shallower "shoulder". The shallower shape is close to $k_h^{-5/3}$, as one would expect for a forward energy cascade range simply on dimensional arguments (a la Kolmogorov). When the horizontal velocity is decomposed into geostrophic and ageostrophic components (*e.g.,* the Helmholtz decomposition in *Stratified Turbulence*), it shows a dominance of the geostrophic velocity on larger scales (where the spectrum is steep) and ageostrophic velocity on smaller scales (where it is shallow). This is consistent with the argument at the start of this section about how the enstrophy range in geostrophic turbulence develops its own dynamical inconsistency.

More physically realistic posings of the submesoscale transition problem have turbulence generated by instability of the mean circulation. In Capet *et al.* (2008b) an oceanic eastern boundary region is forced by a mean equatorward wind stress in a configuration that mimics the California Current System. This develops a baroclinically unstable alongshore flow and mesoscale eddies and, at high enough resolution and Re values, a spontaneous outbreak of submesoscale currents. In this regime the submesoscale flow is strongest near the surface, and it arises primarily through

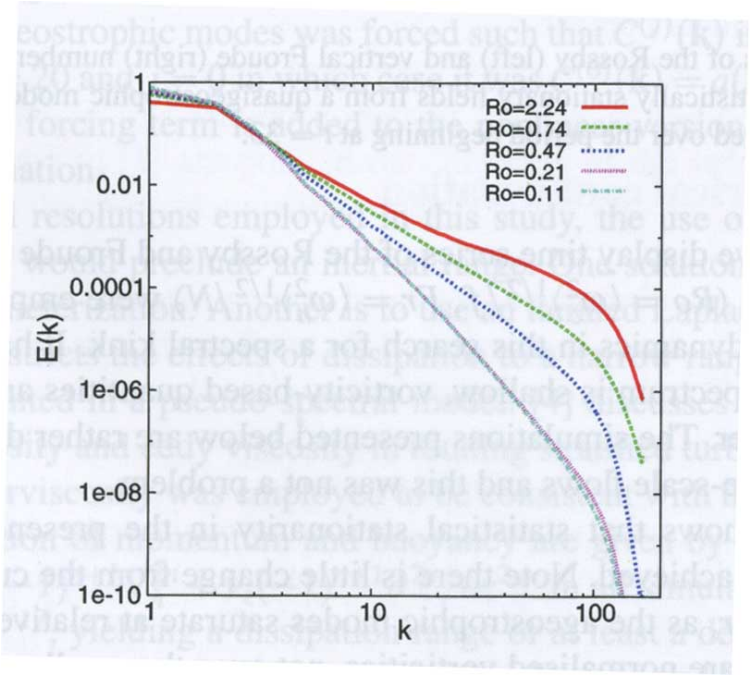

Figure 20: The horizontal energy spectrum at various Rossby numbers Ro in a randomly forced flow using the Boussinesq equations. Notice the progressive shallowing of the spectrum at high wavenumbers with increasing Ro. The forcing is at a large-scale in $\mathbf{k}_h$ and intermediate-scale in k_z. Ro is defined as r.m.s. vertical vorticity divided by f. (Bartello, 2010)

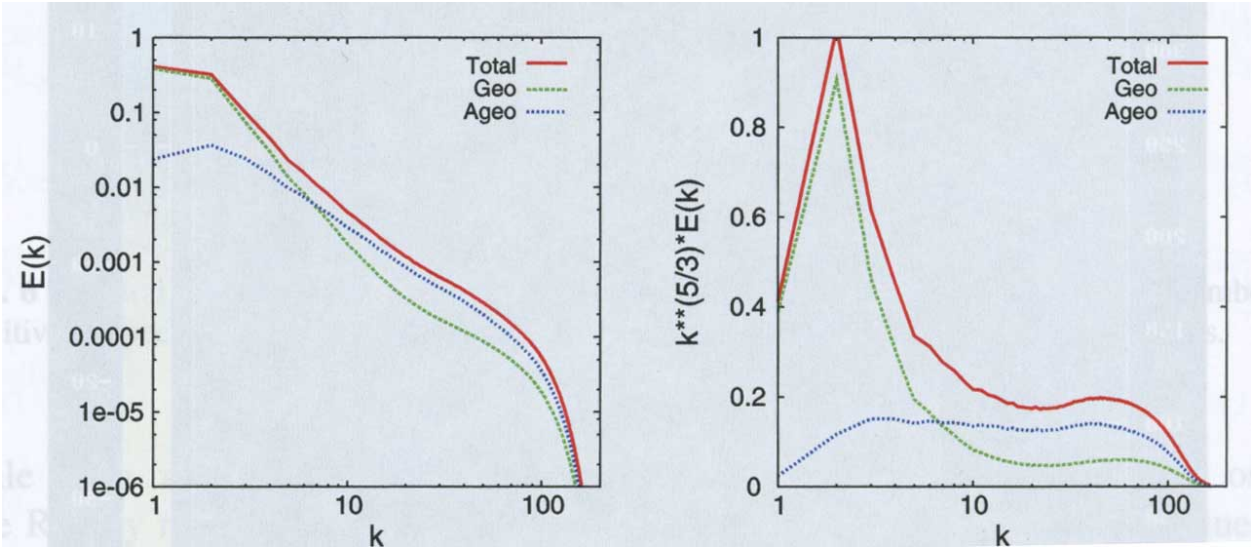

Figure 21: The total energy spectrum of the simulation in Fig. 20 with the highest Ro value, along with its decomposition into contributions from geostrophic and ageostrophic modes. Left: the usual log-log plot; Right: a linear-log plot compensated by $k^{5/3}$. Ageostrophic modes are dominant at high k where the forward enstrophy cascade of QG has changed into a forward energy cascade with approximately Kolmogorov-like inertial range scaling in spite of significant anisotropy due to rotation and stable stratification. (Bartello, 2010)

frontogenesis of surface buoyancy gradients acted on by the high horizontal strain rate between mesoscale eddies. A snapshot of the vertical vorticity is in Fig. 22, where the submesoscale fronts are evident in the wiggly lines of high cyclonic vorticity. A similarly posed problem for the Peruvian Current system also shows spontaneous submesoscale currents (Fig. 23). In this flow configuration, they more have the structure of cold filaments than fronts, and the filamentary flows are themselves unstable and generate spiral vortices. A third example is Eady's flow (*i.e.,* a mean flow with $\overline{\mathbf{u}} = Szb\hat{f}x$), whose baroclinic instability generates first mesoscale eddies then submesoscale fronts and finally frontal instabilities through their horizontal shear (Molemaker *et al.*, 2010).

The energy spectra in these flows with submesoscale regime transitions seem to have $E(k) \sim k_h^{-2}$ or $k_h^{-5/3}$, hence a scale-local Rossby number Ro_L that increases as L decreases, ultimately arriving at a high degree of dynamical inconsistency with the QG approximation. The latter spectrum shape is the same as what arises in the purely stratified problem on scales larger than V/N (Lindborg, 2006, discussed in *Stratified Turbulence*). This suggests that there may be a rather seamless transition in the forward energy cascade from the rotationally influenced submesoscale into the non-rotational stratified regime, although as yet there is no simple theory for this type of behavior. Because frontogenesis and filamentogenesis seems to be important processes in the examples to date, some additional interest has developed in SQG turbulence since it shows some aspects of this behavior; however, as discussed in the preceding section, SQG by itself is incapable of completing the route to dissipation and is only a partial model for submesoscale dynamics. This subject is an exciting, new scientific frontier in geophysical turbulence in the regime with $Ro, Fr = \mathcal{O}(1)$.

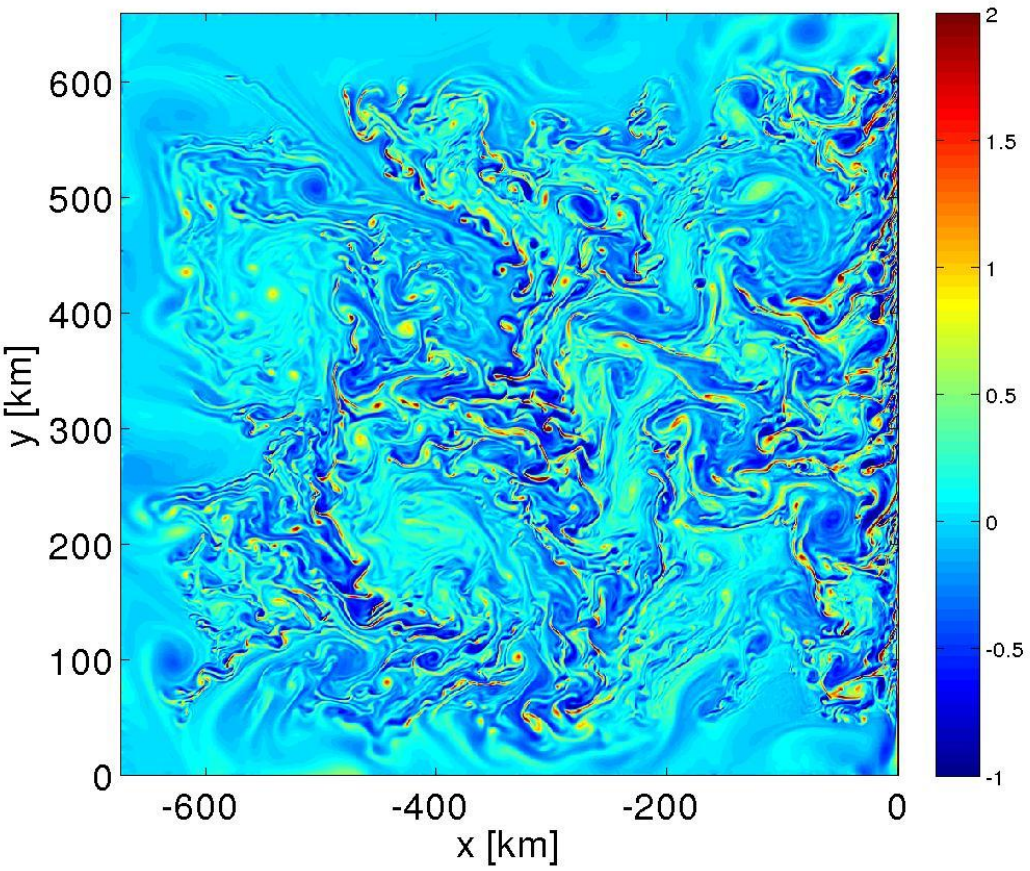

Figure 22: Snapshot of surface vertical vorticity ζ^z normalized by f in an idealized Eastern Boundary Current with equatorward wind stress. Intense submesoscale activity — fronts, frontal instabilities, and coherent vortices — occurs near the boundary and surrounding the mesoscale eddy centers. (Capet *et al.*, 2008b)

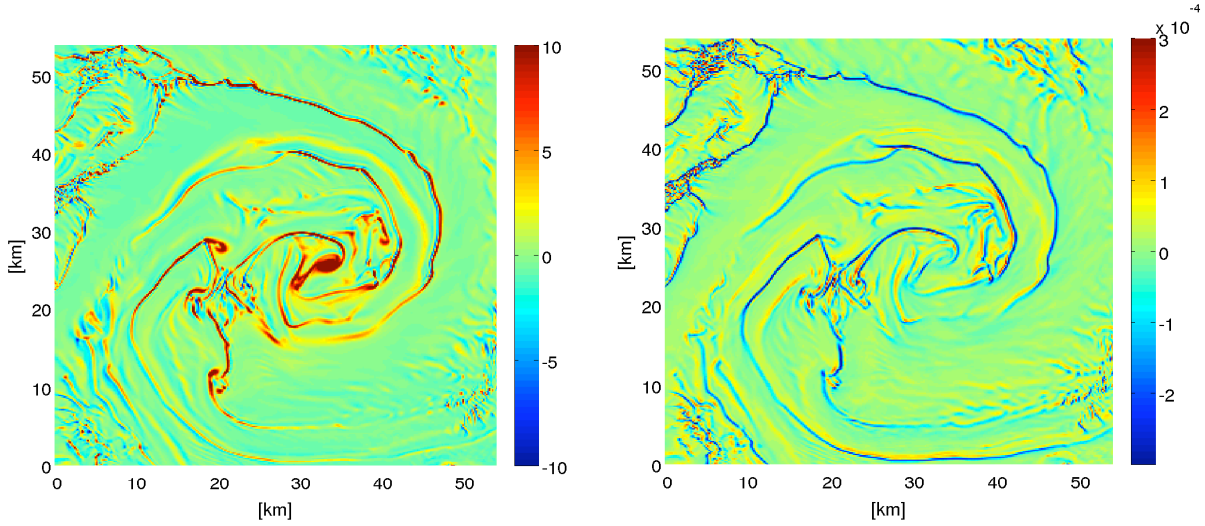

Figure 23: Snapshot of a subdomain from a regional simulation of the upwelling circulation off Peru showing a submesoscale surface cyclonic spiral vortex with frontal and filamentary arms seen in ζ^z/f (top) and w (bottom) in a near-surface horizontal plane. Notice the mixture of two-signed frontal and one-signed filamentary lines in the secondary circulation outside the vortex core. (McWilliams, 2010, with thanks to Francois Colas)

10 Submesoscale Emergence in Oceanic General Circulation

For the most part GCMs are configured on the global scale with whatever spatial resolution is feasible. This does a good job of encompassing the geostrophic dynamics of synoptic and mesoscale eddies, along with many other processes, but it may not adequately represent the submesoscale transition discussed in Sec. 9. An alternative approach is to used embedded high-resolution grids in subdomains of coarser-resolution large-domain models, *e.g.,* a zoom in on the Gulf Stream region within the Atlantic Ocean. Such a case is shown in Fig. 24, where it is clear that there is a great deal of submesoscale activity in the strongest currents as well as the more quiescent mesoscale background flows.

In this context a horizontal wavenumber spectrum and rotational-divergent decomposition of the horizontal surface velocity (Figs. 25-26) shows that there is a flattening of the spectrum slope at smaller scales (as in Fig. 20), mainly due the strengthening of the divergent (ageostrophic) component. Recall the Helmholtz decomposition for a horizontal velocity vector,

$$\mathbf{u}_h = \mathbf{u}_r + \mathbf{u}_d = \hat{\mathbf{z}} \times \nabla_h \psi + \nabla_h \chi \,. \tag{70}$$

As k_h increases — here beyond an inverse wavelength of $\lambda \approx 30$ km — the divergent component is no longer safely small compared to the rotational component, QG dynamics are not an adequate dynamical model, and a forward energy cascade can arise. In particular, this is further support for the proposition that QG dynamics — like small Fr stratified turbulence at high k_h — contains the seeds of its own inconsistency, hence invalidity, when there is a wavenumber spectrum shallower than k_h^{-3} with an increasing local Ro value with increasing k_h.

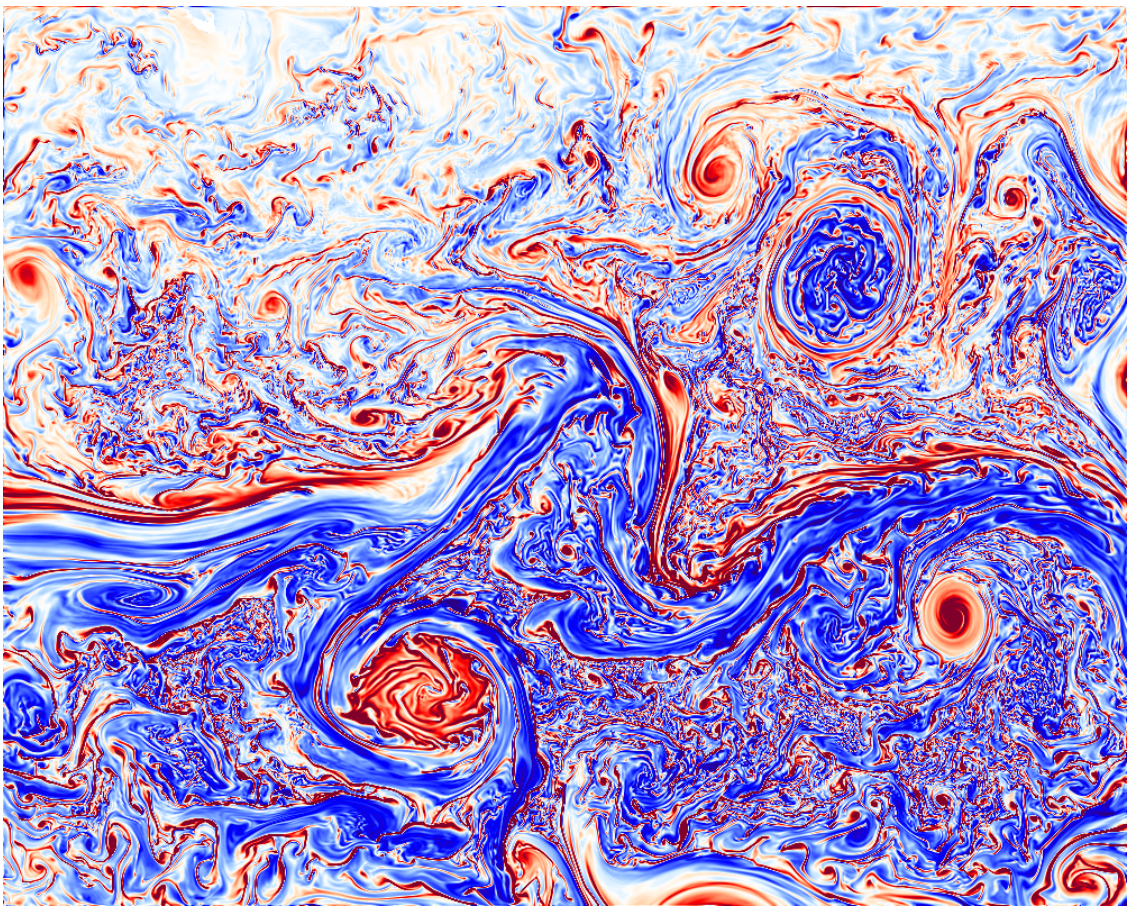

Figure 24: Snapshot of vertical vorticity ζ^z at the surface in a nested-grid simulation of the Gulf Stream in the offshore region downstream from its separation from the western boundary. The plotted domain is about 1000 km X 800 km. The principle phenomena are the following: a meandering eastward jet through the central latitudes with positive (red) vorticity on its north side and negative (blue) on its south side; big (mesoscale) Ring vortices that have pinched off from large meanders, cyclonic in the south and anticyclonic in the north; and abundant submesoscale activity arising from frontogenesis and instabilities of the larger currents that have quite different structures in different flow and stratification sectors of the flow. This is from a simulation using the Regional Oceanic Modeling System here at UCLA. (Gula *et al.*, 2014)

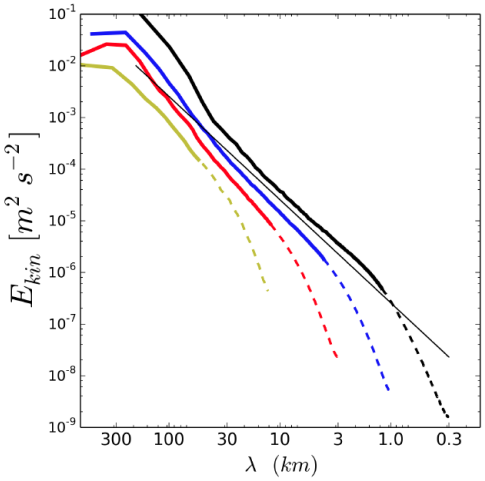

Figure 25: Horizontal kinetic energy spectra $E_{kin}(k_h)$ at the surface averaged over many different snapshots in the post-separation sector of the Gulf Stream and over the horizontal wavenumber direction (*i.e.,* azimuthally). The different curves are for different model grid resolutions, *viz.,* $dx =$ 6, 1.5, 0.5, and 0.15 km, and the abscissa is wavelength $\lambda = 2\pi/k_h$. The dashed lines indicate the model's dissipation range due to the subgrid-scale diffusion employed. The thin reference line has a shape of k_h^{-2}. As the resolution increases, the spectrum fills out toward smaller scales with a shape inconsistent with the enstrophy cascade range in homogeneous geostrophic turbulence, reflecting the emergence of submesoscale surface-layer currents with partly ageostrophic dynamics.

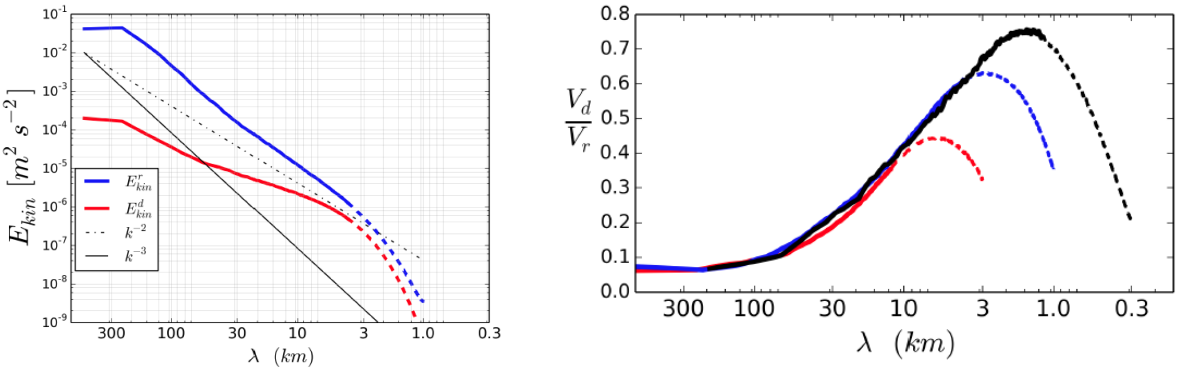

Figure 26: (Top) Horizontal kinetic energy spectra at the surface averaged over many different snapshots in the post-separation sector of the Gulf Stream from a simulation with $dx = 0.5$ km.. The blue curve is for the rotational component $\mathbf{u}_r$, and the red curve is for the divergent component $\mathbf{v}_d$ in a Helmholtz decomposition. With decreasing λ the divergent energy fraction approaches the rotational one, especially in the $\sim\ k_h^{-2}$ submesoscale range before the onset of the dissipation range. (Bottom) The same results plotted as the velocity component ratio, $V_d/V_r = (E_d/E_r)^{1/2}$, for grid resolutions of $dx = 1.5$, 0.5, and 0.15 km. Quasigeostrophic theory would predict this ratio to be small and $\mathcal{O}(Ro)$, even uniformly so with k_h in an enstrophy cascade range. Here the ratio is increasing with k_h indicating decreasing consistency with QG theory.

References

Andrews, D.G., J.R. Holton, and C.B. Leovy, 1987: *Middle Atmosphere Dynamics*. Academic Press.

Arbic, B.K., and G.R. Flierl, 2004: Baroclnically unstable geostrophic turbulence in the limits of strong and weak bottom friction: Application to midocean eddies. *J. Phys. Ocean.* **34**, 2257-2273.

Bartello, P., 2010: Quasigeostrophic and stratified turbulence in the atmosphere. In: *IUTAM Symposium on Turbulence in the Atmosphere and Oceans*, D. Dritschel, ed., Springer, 117-130.

Blumen, W., 1978: Uniform potential vorticity flow: Theory of wave interactions and two-dimensional turbulence. *J.Atmos. Sci.* **35**, 774-783.

Bretherton, F.P., and D.B. Haidvogel, 1976: Two-dimensional turbulence above topography. *J. Fluid Mech.* **78**, 129-154.

Capet, X., P. Klein, B.L. Hua, G. Lapeyre, and J.C. McWilliams, 2008a: Surface kinetic energy transfer in SQG flows. *J. Fluid Mech.* **604**, 165-175.

Capet, X., J.C. McWilliams, M.J. Molemaker, and A. Shchepetkin, 2008b: Mesoscale to submesoscale transition in the California Current System: Flow structure, eddy flux, and observational tests. *J. Phys. Ocean* **38**, 29-43.

Charney, J.G., 1971: Geostrophic turbulence. *J.Atmos. Sci.* **28**, 1087-1095.

Davidson, P.A., P.J. Staplehurst, and S.B. Dalziel, 2006: On the evolution of eddies in a rapidly rotating system. *J. Fluid Mech.* **557**, 135-144.

Eady, E.T., 1949: Long waves and cyclone waves. *Tellus* **1**, 33-52.

Ferrari, R., J.C. McWilliams, V.M. Canuto, and M. Dubovikov, 2008: Parameterization of eddy fluxes near oceanic boundaries. *J. Climate* **21**, 2770-2789.

Galperin, B., S. Sukoriansky, and N. Dikovskaya, 2008: Zonostrophic turbulence. *Physica Scripta* **T132**, 014034, 1-7.

Gent, P.R., and J.C. McWilliams, 1990: Isopycnal mixing in ocean circulation models. *J. Phys. Ocean.* **20**, 150-155.

Graves, L.P., J.C. McWilliams, and M.T. Montgomery, 2006: Vortex evolution due to straining: A mechanism for dominance of strong, interior anticyclones. *Geophys. & Astrophys. Fluid Dyn.* **100**, 151-183.

Gula, J., M.J. Molemaker, and J.C. McWilliams, 2014: Submesoscale cold filaments in the Gulf Stream. *J. Phys. Ocean.* **44**, 2617-2643.

Haidvogel, D.B., and P.B. Rhines, 1983: Waves and circulation driven by oscillatory winds in an idealized ocean basin. *Geophys. Astrophys. Fluid Dyn.* **25**, 1-63.

Held, I., R. Pierrehumbert, S. Garner,and K. Swanson, 1995: Surface quasi-geostrophic dynamics. *J. Atmos. Sci.* **282**, 1-20.

Holloway, G. (1992), Representing topographic stress for large-scale ocean models, *J. Phys. Ocean.*, *22*, 1033–1046.

Hoskins, B., and F.P. Bretherton, 1972: Atmospheric frontogenesis models: Mathematical formulation and solution. *J. Atmos. Sci.* **29**, 11-37.

Hoyer, J., and R. Sadourny, 1982: Closure modeling of fully developed baroclinic instability. *J. Atmos. Sci.*, **39**, 707-721.

Kloosterziel, R.C., and G.F. Carnevale,, 2008: Vertical scale selection in inertial instability *J. Fluid Mech.* 594, 249-269.

Lapeyre, G. and Klein, P., 2006: Dynamics of the upper oceanic layers in terms of surface quasigeostrophy theory. *J. Phys. Ocean.* **36**, 165-176.

Larichev, V.D., and J.C. McWilliams, 1991: Weakly decaying turbulence in an equivalent-barotropic fluid. *Phys. Fluids A* **3**, 938-950.

Lindborg, E., 2006: The energy cascade in a strongly stratified fluid. *J. Fluid Mech.* **550**, 207-242.

Lorenz, E., 1967: *The Nature and Theory of the General Circulation of the Atmosphere*. World Meteorological Organization, Geneva.

Majda, A., and E.G. Tabak, 1996: A two-dimensional model for quasigeostrophic flow: comparison with the two-dimensional Euler flow. *Physica D* **98**, 515-522.

McEwan, A., 1976: Angular momentum diffusion and the initiation of cyclones. *Nature* **260**, 126-128.

McWilliams, J.C., and J.H.S. Chow, 1981: Equilibrium geostrophic turbulence: I. A reference solution in a β-plane channel. *J. Phys. Ocean.* **11**, 921-949.

McWilliams, J.C., 1984: The emergence of isolated, coherent vortices in turbulent flow. *J. Fluid Mech.* **146**, 21-43.

McWilliams, J.C., J.B. Weiss, and I. Yavneh, 1994: Anisotropy and coherent structures in planetary turbulence. *Science* **264**, 410-413.

McWilliams, J.C., 2006: *Fundamentals of Geophysical Fluid Dynamics*. Cambridge University Press, Cambridge.

McWilliams, J.C., 2010: A perspective on submesoscale geophysical turbulence. In: *IUTAM Symposium on Turbulence in the Atmosphere and Oceans*, D. Dritschel, ed., Springer, 131-141.

Molemaker, M.J., J.C. McWilliams, and X. Capet, 2010: Balanced and unbalanced routes to dissipation in an equilibrated Eady flow. *J. Fluid Mech.* **654**, 35-63.

Nozawa, T., and S. Yoden, 1997: Formation of zonal band structure in forced two-dimensional turbulence on a rotating sphere. *Physics of Fluids* **9**, 2081-2093.

Panetta, R.L., 1993: Zonal jets in wide baroclinically unstable regions: Persistence and scale selection. *J. Atmos. Sci.* **50**, 2073-2016.

Plumb, R.A., and R. Ferrari, 2005: Transformed Eulerian-mean theory. I: Non-quasigeostrophic theory for eddies on a zonal mean flow. *J. Phys. Ocean.* **35**, 165-174.

Polvani, L.M., J.C. McWilliams, M.A. Spall, and R. Ford, 1994: The coherent structures of Shallow-Water turbulence: Deformation-radius effects, cyclone/anticyclone asymmetry, and gravity-wave generation. *Chaos* **4**, 177-186.

Rhines, P.B., 1975: Waves and turbulence on the β-plane. *J. Fluid Mech.* **69**, 417-443.

Rhines, P.B., 1979: Geostrophic turbulence. *Ann. Rev. Fluid Mech.* **11**, 401-441.

Roullet, G., J.C, McWilliams, X. Capet, and N.J. Molemaker, 2011: Properties of equilibrium geostrophic turbulence with isopycnal outcropping. *J. Phys. Ocean.*, submitted.

Salmon, R. (1982), Geostrophic turbulence, *Topics in Ocean Physics*, Proc. Int. Sch. Phys. 'Enrico Fermi', Varenna, Italy, 30–78.

Scott, R.K., and L.M. Polvani, 2008: Equatorial super-rotation in shallow atmospheres. *Geophys. Res. Lett.* **35**, L24202.

Sen, A., R.B. Scott, and B.K. Arbic, 2008: Global energy dissipation rate of deep-ocean low-frequency flows by quadratic bottom boundary layer drag: Computations from current meter data. *Geophys. Res. Lett.* **35**, L09606.

Smith, L.M., and F. Waleffe, 1999: Transfer of energy to two-dimensional large scales in forced, rotating three-dimensional turbulence. *Physics of Fluids* **11**, 1608- .

Treguier, A.M., and J.C. McWilliams, 1990: Topographic influences on wind-driven, stratified flow in a β-plane channel: An idealized model of the Antarctic Circumpolar Current. *J. Phys. Ocean.* **20**, 324-343.

Treguier, A.M., and R.L. Panetta, 1994: Multiple zonal jets in a quasigeostrophic model of the Antarctic Circumpolar Current. *J. Phys. Ocean.* **24**, 2263-2277.

Williams, G.P., 1978: Planetary circulations: Barotropic representation of Jovian and terrestrial turbulence. *J. Atmos. Sci.* **35**, 1399-1424.

Wolff, J.O., E. Maier-Reimer, and D.J. Olbers, 1991: Wind-driven flow over topography in a zonal β-plane channel: A quasigeostrophic model of the Antarctic Circumpolar Current. *J.Phys.Ocean.* **21**, 236-264.